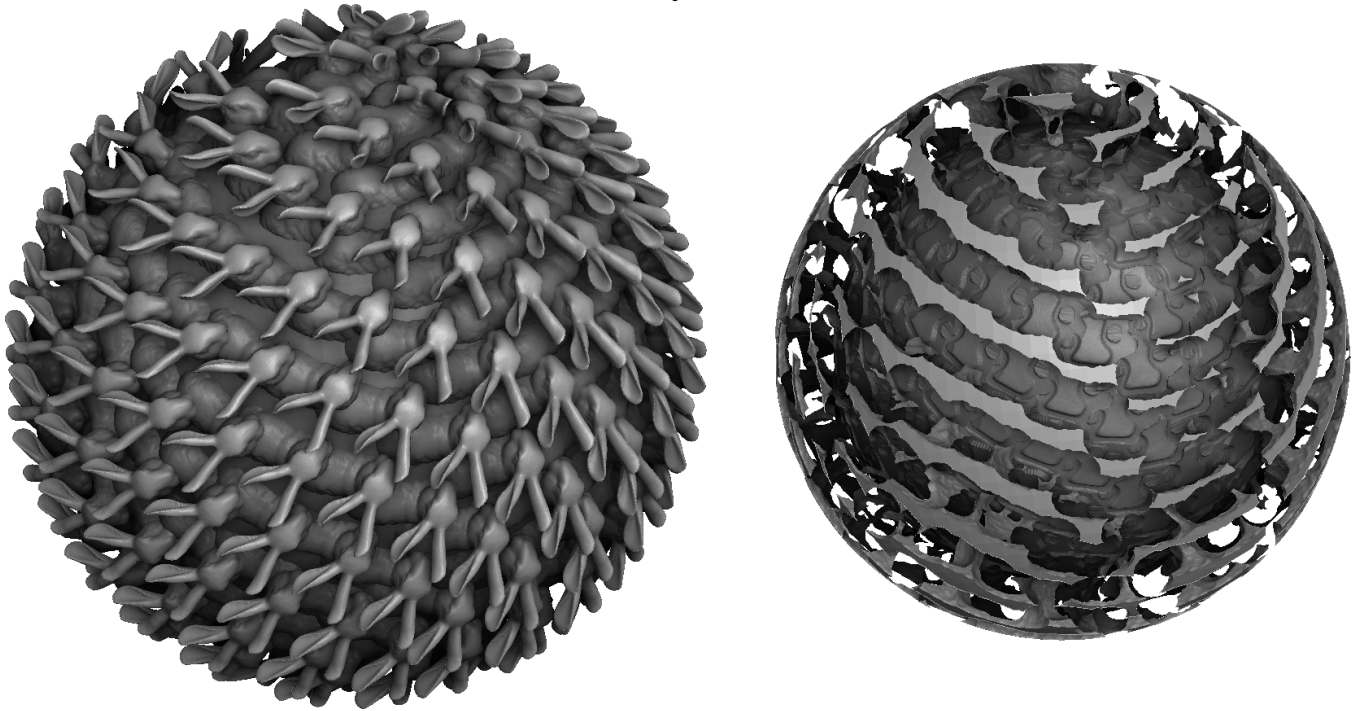


Exact predicates, exact constructions and combinatorics for mesh CSG.

Bruno Lévy, Inria Saclay, Université Paris Saclay, CNRS, Labo. de Maths. d'Orsay

Bruno.Levy@inria.fr



Union and difference between a Fibonacci distribution of 200 bunnies and a sphere (30 million facets in total).

ABSTRACT

This article introduces a general mesh intersection algorithm that exactly computes the so-called Weiler model and that uses it to implement boolean operations with arbitrary multi-operand expressions, CSG (constructive solid geometry) and some mesh repair operations. From an input polygon soup, the algorithm first computes the co-refinement, with an exact representation of the intersection points. Then, the decomposition of 3D space into volumetric regions (Weiler model) is constructed, by sorting the facets around the non-manifold intersection edges (radial sort), using specialized exact predicates. Finally, based on the input boolean expression, the triangular facets that belong to the boundary of the result are classified. This is, to our knowledge, the first algorithm that computes an exact Weiler model. To implement all the involved predicates and constructions, two geometric kernels are proposed, tested and discussed (arithmetic expansions and multi-precision floating-point). As a guiding principle, the combinatorial information shared between each step is kept as simple as possible. It is made possible by treating all the particular cases in the kernel. In particular, triangles with intersections are remeshed using the (uniquely defined) Constrained Delaunay Triangulation, with symbolic perturbations to disambiguate configurations with co-cyclic points. It makes it easy

to discard the duplicated triangles that appear when remeshing overlapping facets. The method is tested and compared with previous work, on the existing “thingi10K” dataset (to test co-refinement and mesh repair) and on a new “thingiCSG” dataset made publicly available (to test the full CSG pipeline) on a variety of interesting examples featuring different types of “pathologies”.

1 INTRODUCTION AND PREVIOUS WORK

1.1 Why is mesh intersection so hard ?

Mesh intersection is a classical operation in geometry processing. It is the basic component of higher-level operations, such as boolean operations, constructing solid geometry, mesh repair, mesh cleaning, or volumetric modelling operations. However, it is still an important source of difficulties when implementing geometry processing systems, and it is still an active area of research and development. At first sight, it may seem rather surprising, because the problem looks simple: from a mathematical point of view, what we want to construct is clearly defined. The input is a set of triangulated surfaces, with possibly intersecting, or even overlapping/coplanar triangles. The desired output is another set of triangles, that represent exactly the same surfaces, but that have no intersection. So

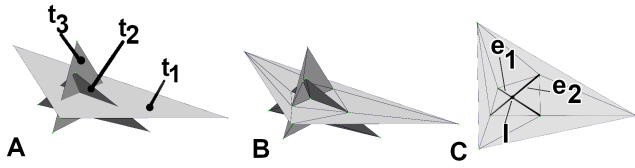


Figure 1: Intersection between three triangles

why don't we simply "implement the math"? Why don't we have a standard implementation that everybody uses? Why is there still active research on this topic, that is several decades old? The main difficulty is caused by the representation of coordinates in the computer. Floating point numbers have a limited precision, which causes two difficulties:

Geometric predicates: We will need to determine whether a pair of triangles have an intersection, which in turn depends on more "elementary questions", such as whether a point is above or below a plane (in a certain sense). Such "elementary questions", called *predicates*, are functions that take as an argument a (small) number of points (or simple geometric objects) and that returns a set of discrete values. For instance, consider four points p_1, p_2, p_3, p_4 . One may want to know the position of p_4 relative to the supporting plane of p_1, p_2, p_3 , that can be one of ABOVE, BELOW, ON_PLANE. These predicates are the "neuralgic" point of mesh intersection methods: if at one moment the algorithm "thinks" that p_4 is above the supporting plane of p_1, p_2, p_3 , it is important that at another moment the predicate does not say that p_4 is below the same plane. How could this happen? In fact, these predicates can be expressed as the sign of a polynomial in the coordinates of the points, and due to the limited precision of floating point numbers, the output of the predicate can be different from the exact mathematical result, especially around zero, and it can depend on the order of the points: in floating point arithmetic, imagine you compute $(x_1 + x_2) + x_3$, where $x_1 = 1e30, x_2 = 1e - 6$ and $x_3 = -1e30$ (the result should be $1e - 6$). When the computer first evaluates $x_1 + x_2$, it gets $1e30$ (because x_2 is too small relative to x_1), and in the end you get 0. Now if you compute $(x_1 + x_3) + x_2$, you will get a different result ($1e - 6$). Because of that, you may obtain a different result when you ask for the position of p_4 relative to the supporting plane of p_1, p_2, p_3 or when you ask for the position of p_4 relative to p_3, p_2, p_1 ! It can have catastrophic consequences, such as generating an incorrect mesh.

Representing intersections: Once the intersecting triangles are determined, one needs to compute the actual intersection. In general, the coordinates of the intersection between triangles can be expressed as rational fractions (ratios of polynomials in the initial mesh coordinates). Again, in general, they cannot be exactly represented by floating-point numbers. It has several consequences: first, imagine you know the exact coordinates of all the vertices of your mesh, when you convert them into floating point numbers, they will move a little bit. If you do not take care, it may generate new intersections! The problem of constraining the intersection points to have floating-point coordinates is referred to as "snap rounding". It requires special care, that is, one needs to ensure the

output with floating-point coordinates does not have new intersection and is topologically equivalent (in a certain sense) to the exact result [8]. Second, during the computation, one may need to query geometric predicates on the points resulting from intersections, and the answers of these predicates need to be coherent with all the rest! For instance, consider a triangle t_1 that has some intersections with other triangles t_2, \dots, t_n . These intersections create segments e_1 and e_2 in t_1 , and one needs to re-triangulate t_1 in a way that conforms with these segments. In other words, one needs to compute a 2D constrained triangulation in t_1 . This 2D constrained triangulation depends on a set of predicates, and these predicates need to be coherent with all the rest. In fact, the situation is even more complicated: as shown in Figure 1-A, consider that t_1 is a triangle that have intersections with two other triangles t_2 and t_3 , mutually intersecting. The mesh resulting from the intersection of the three triangles is shown in Figure 1-B. When remeshing t_1 , there will be two segments e_1 and e_2 (highlighted in Figure 1-C), (one that corresponds to $t_1 \cap t_2$ and the other one to $t_1 \cap t_3$, that create a new intersection I). Now think of what you have to do to compute this intersection: the extremities of e_1 and e_2 are intersections between input mesh triangles, and we need to compute their intersection. In this specific case, one can compute instead the intersection between the supporting planes of the three triangles (that solely depend on the input points), as will be explained later, but one needs to keep in mind that the intersection I is a constructed points with coordinates that are rational fractions, that will be later passed through the geometric predicates when computing the constrained triangulation of t_1 . Predicates that depend on constructed points are also used in the subsequent steps of the algorithm, such as the "radial sort" operation involved in the construction of the Weiler model, that needs new predicates, as shall be seen later.

Software design questions: geometry or combinatorics? A mesh intersection / mesh CSG system typically takes the form of a pipeline composed of several steps (such as *detect candidate triangles intersections, compute triangle intersections, constrained Delaunay triangulation, merge mesh, classify intersections, simplify*). There are some impactful decisions to take regarding the way these steps communicate, in particular, there are two types of information:

- *geometry*, that is, the exact coordinates of the input points and the constructed intersection points;
- *combinatorics*, that is, a set of index-based (or pointer-based) data structures that store the connections between the triangles (or between some higher-level notions such as charts, shells, regions ...).

In our context, all point coordinates are exactly represented. As a consequence, the two types of information are redundant: at any time one could totally reconstruct the combinatorial information from the sole list of triangles and the (exact) coordinates of their vertices. Hence, the stored combinatorial information either corresponds to the (transient) internal state of one stage (for instance, a Constrained Delaunay Triangulation), or it is a "cache" shared by two stages (or more), ensuring that the stage(s) downstream do not need to recompute some already known combinatorial information.

Then it would be tempting to always keep all the combinatorial information. However, doing so has the hidden cost of making the architecture more complicated and more difficult to test. There is

a tradeoff to find between a set of independent and easy-to-test pipeline stages connected by a simple communication protocol, or a fully interconnected set of pipeline stages, (slightly) more efficient, but (considerably) harder to design, to test and to debug.

1.2 Summary of this article’s contributions

This article introduces the first algorithm that computes the so-called Weiler model [50] *exactly*, that is, a data structure that stores the decomposition of 3D space into volumetric regions yielded by a set of (possibly intersecting) triangulated surfaces.

The algorithm is based on several components:

- a multi-thread friendly constrained Delaunay triangulation;
- an algorithm to construct the Weiler model;
- a (mostly) combinatorial classification algorithm that extracts from the Weiler model the boundary of a region described by an arbitrary boolean expression;
- an algorithm to simplify the triangulation of co-planar regions.

To implement the required exact predicates and exact constructions, two geometric kernel are described and analyzed:

- one is based on arithmetic expansions, like in the approach proposed by Shewchuk for predicates [37], with the difference that arithmetic expansions are also used to store constructed points;
- the other one is based on multi-precision arithmetics.

For both geometric kernels, I explain how to efficiently implement the arithmetic filters, the predicates, and the symbolic perturbations that ensure the uniqueness of the constrained Delaunay triangulation.

The algorithm is tested and compared with previous work on two databases:

- The Thingi10K database [52], used to evaluate the co-refinement algorithm;
- A new ThingiCSG database with a collection of CSG trees, and the skeleton of an OpenSCAD-compatible CSG engine that can be used to test and benchmark future works¹.

This algorithm produces the co-refinement or the result of a boolean operation applied to a set of input meshes, with all intersection points exactly represented. In the frame of this article, I do not address the (difficult) problem of converting these exact points into standard floating-point coordinates while preserving some topological properties (snap rounding). The reader is referred to [8, 47] for an extensive description of snap rounding as well as a possible algorithm.

1.3 Previous work on mesh intersection

Low level (arithmetics). At the early times, standard floating point numbers were used, with some carefully tuned threshold and tolerances to detect corner cases. In the context of tetrahedral meshing, when checking the validity of a mesh element, it is possible to avoid the arithmetic cancellation problem mentioned in the introduction by testing all the permutation of the element’s vertices. From the early 90’s to now, spectacular results were obtained using the type of strategy mentioned above, and deployed

in challenging industrial settings such as highly anisotropic mesh adaptation for ultrasonic flows [11, 28]. Another possibility consists in trying to “simply implement the math”, in other words, pushing the difficulties towards the predicates [37, 39], by ensuring that they exactly follow the definition of the mathematical predicate. How is it possible with a computer? Remember, geometric predicates are polynomials in coordinates of the input mesh’s vertices. The idea in Shewchuk’s work is to use arithmetic expansions, that is, a point coordinate will be represented by an array of floating point numbers x_1, x_2, \dots, x_N (instead of a single floating point number). The represented number corresponds to the sum of all the numbers in the array. Moreover, these numbers are sorted by decreasing exponents, and are well separated. That is, the sum $x_2 + x_3 + \dots + x_N$ is smaller than the floating point value of the least significant bit of x_1 . As a consequence, the sign of the represented number is completely determined by the sign of x_1 . It is possible to implement addition, subtraction and multiplication for expansions. If the processor supports the fused multiply-add instruction `fma` (which is the case of most modern processors), some noticeable performance gain will be obtained (one of the basic operations, `two_product()` takes 2 instructions with `fma` versus 13 instructions if `fma` is not available). However, even with `fma`, operations on expansions are 40 to 100 times slower than with standard double-precision numbers. For this reason, several strategies were developed to quickly give the answer in the easy cases. Shewchuk developed an adaptive precision algorithm, that computes the most significant elements and refines as needed whenever the sign cannot be determined. However, this strategy is delicate to implement².

It is also possible to use interval arithmetics, that is, implementing addition, subtraction and product for `low,high` pair of floating point numbers. Each time 0 is not contained in the `[low,high]` interval, the sign of the represented number is known. In all other cases, one needs to relaunch the computation with expansions. Since it does not happen often, there is a significant performance gain. Another possibility to quickly determine the sign in the easy configurations is to use arithmetic filters [33]. The idea shares some similarities with interval arithmetics, with the difference that it computes with the estimated number an error bound, using a combination of static information (deduced from the algebraic expression to be computed) and dynamic information (computed from the actual values passed to the expression). The *Predicate Construction Kit* [23] takes an algebraic expression of the predicate, and generates the filter with *FPG* [33], the code that computes it with expansions when the filter fails, as well as symbolic perturbations [10] for the degenerate configurations (such as 4 cocyclic points in a Delaunay triangulation). It was used to generate the non-standard predicates required to compute the intersection between a Voronoi or a power diagram and a surface or a volume embedded in n dimensions, used in semi-discrete optimal transport [22] and its applications in fluid simulation [30] and cosmology [24, 35, 48].

High Level (intersections and data structures). Using these technologies, algorithms and softwares were developed for robust tetrahedral meshing of triangle soups (that may have intersections), first in the TetWild package [15] that was improved and made

¹see links at the end of this article

²One may think of an automatic code generator for that.

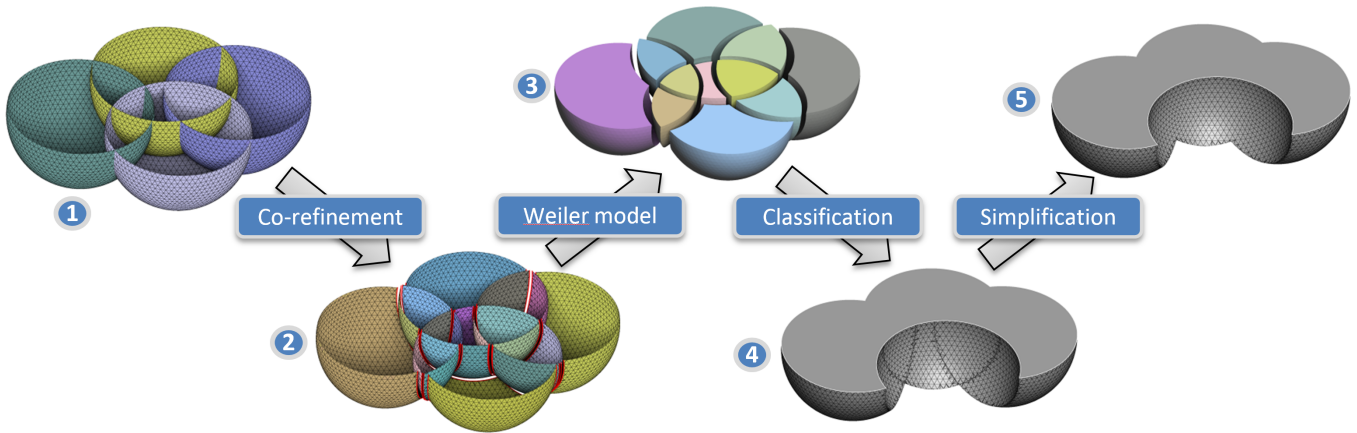


Figure 2: Overview of the algorithmic pipeline for computing boolean operations. From a set of intersecting triangulated surfaces (1), we first compute the co-refinement (2), then the Weiler model with all volumetric relations (3), from which the result of the boolean operation is extracted - here the union of three spheres minus the fourth one (4). Finally, the mesh is simplified by merging co-planar triangles (5).

more efficient a while later, based on a more sophisticated algorithm, dubbed as FastTetWild [14]. In the same period of time, the Thingi10K dataset was published [52]. It provides the research community with a large database of meshes, with many different cases of degeneracies and inconsistencies. It represents an excellent stress test for mesh intersection algorithms. With objectives and ideas similar to the *Predicate Construction Kit* [23] a system for indirect predicates was introduced [1], with in addition the idea of storing intermediate construction (that is, new points generated during the execution of the algorithm). Based on this system, a series of significant advances was published, first to compute mesh arrangements [4] then boolean operations [5]. Both methods need to compute constrained triangulations. For that, a highly efficient (linear complexity) ear cutting algorithm was proposed [27]. The idea of indirect predicates was also used to implement 3D constrained Delaunay triangulation [9], based on an exact representation of the Steiner points.

To help structuring the information through the processing pipeline, several combinatorial data structures were proposed, such as the Weiler model [49]. This data structure is popular in computational geosciences, where it is used to represent the volumetric relations between rock layers and geologic faults [3, 20, 32, 36, 42]. It constructs relations between volumes from intersecting surfaces by sorting triangles around non-manifold intersection edges. We shall see later in this article how this operation can be *exactly* implemented. To study the combinatorial aspects of the algorithms, I shall use the notations of combinatorial maps [25]. Based on an algebraic specification, the notion of combinatorial maps is well suited to mathematically define the operations of a 3D modeler [2], as well as multiresolution modeling operators [18] and some operations involved in hexahedral mesh generation [29]. In our context, it facilitates describing and implementing the algorithms in a readable and compact way.

OpenSCAD and its three geometric kernels. The OpenSCAD software [51] is a scriptable CAD package widely used in the fabrication community. It is based on the CGAL computational geometry library [45], more precisely, it uses the implementation of Nef complexes [12] available in CGAL. To improve computation time, an alternative algorithm, based on co-refinement, was implemented, also in CGAL [16]. It is significantly faster than the initial implementation (10x to 50x). All the approaches mentioned above follow the exact geometry paradigm (exact predicates and exact constructions, except for the final conversion to floating-point coordinates / snap rounding). There exists a worth mentioning original and highly effective alternative to this paradigm: instead of doing all the computations in exact mode then converting into floating-point coordinates while preserving some topological properties, why not doing all computations in floating point coordinates, while ensuring that each individual computation preserves some properties? It is the strategy proposed in [41], that builds a network of predicates and operations of increasing dimensions on top of 1D axis-aligned comparisons (that can be done exactly), while ensuring that the mesh stays manifold at each level. A fine-tuned parallel implementation was developed [19] and integrated as an alternative kernel for OpenSCAD. Since it solely uses single-precision floating point arithmetics, it can also run on the GPU. The performance gain is spectacular (three orders of magnitude). In this article, I follow the more classical approach (exact predicates and exact constructions). I implemented an Open-SCAD compatible software to compare the results with the three geometric kernels mentioned above (§3.2 p.22).

1.4 Overview of this article

The approach presented in this article shares some similarities with the works mentioned above, in particular [4, 5], with the following differences:

- (1) exact constructions are used instead of Predicate Construction Kit or indirect predicates;

- (2) the algorithm computes a constrained *Delaunay* triangulation (CDT), which ensures the uniqueness of the obtained triangulation. The uniqueness of the triangulation is useful to make sure that the same triangles will be generated in configurations with co-planar overlapping facets. Then duplicated triangles can be easily eliminated, whereas previous works need to use an auxiliary data structure to identify overlapping zones. Note that CDT uses the `in_circle` predicates, that depends on 4 points. Using Predicate Construction Kit or indirect predicates would generate a large number of instances of the `in_circle` predicates (depending on whether the points are initial vertices or intersections). Here this “combinatorial explosion” is avoided thanks to the exact constructions. In a certain sense, the complexity is pushed towards the kernel;
- (3) the algorithm computes the 3D partition of space into volumes, represented in a data structure called the Weiler model [49]. I shall explain later how this data structure can be efficiently constructed, and how most of the calls to the predicates can be avoided by exploiting the combinatorics. Then I shall use this data structure to implement boolean operations and CSG primitives, still exploiting the combinatorics as much as possible. To my knowledge, this is the first algorithm that *exactly* computes the Weiler model.

This article introduces an algorithmic pipeline depicted in Figure 2. Given an input polygon soup, the algorithm computes the co-refinement (§2.1 p.5), based on an exact constrained Delaunay triangulation constructed in each facet that has intersections (§2.1.3 p.9). Then, the algorithm creates the Weiler model (§2.2.1 p.13), that represents all the radial relations around the non-manifold intersection edges as well as the volumetric relations between the regions delimited by the surfaces. Finally, from the input boolean expression, a classification algorithm selects the triangular facets that belong to the boundary of the result (§2.2.3 p.15). In addition, an optional step merges and re-triangulates co-planar facets (§2.2.4 p.16). To exactly represent the intersection points, I implemented and tested two different arithmetic kernels (§2.4 p.17). One is based on arithmetic expansions (§2.4.1 p.17), and the other one on multi-precision floating point arithmetics (§2.4.2 p.20). Both are pre-filtered using interval arithmetics. The uniqueness of the Delaunay triangulation is ensured, even in configurations with cocyclic points, by using symbolic perturbations. This ensures that regions overlapped by multiple coplanar input facets are coherently and uniquely triangulated. Finally, I tested the method and compared with previous work (§3 p.21), on the existing “thingi10K” dataset for the co-refinement algorithm, (§3.1 p.21) and on a new “thingiCSG” dataset together with an OpenSCAD compatible CSG engine, both made publicly available³, to test the full CSG pipeline on a variety of interesting examples featuring different types of “pathologies” (§3.2 p.22).

³see links at the end of this article

2 THE ALGORITHM

2.1 Mesh co-refinement

Mesh co-refinement takes as input a set of triangulated surface. No assumption is made regarding the structure of this input. It can be a triangle soup made of disconnected triangles. It can have co-planar facets. Duplicated vertices are pre-detected and merged using spatial sorting. Duplicated facets are then pre-detected and discarded, using lexicographic sort. Then, the different substeps of the algorithm, outlined in Figure 3, are as follows:

- Detect candidate triangle intersection pairs (§2.1.1 p.5);
- Compute triangle intersections (§2.1.2 p.7);
- Re-triangulate the intersected triangles, using a constrained Delaunay triangulation (§2.1.3 p.9)

The output is a valid mesh that exactly represents the same geometry as the input mesh. It is valid in the sense it has no intersection. Output vertices stemming from triangle intersections are exactly represented. We shall see two different ways of doing that, using either arithmetic expansions or multi-precision floating-point numbers (§2.4 p.17).

2.1.1 Detecting candidate intersecting facet pairs. The first step of the algorithm determines all pair of potentially intersecting facets. To avoid having to test the $N_F^2/2$ pairs of triangles, we use the classical AABB data structure (axis-aligned bounding box tree). Readers already familiar with AABBs may skip this subsection. However, I found it useful to give here some details and references, in particular about the idea that an AABB can be stored in compact form, mostly by re-ordering the mesh elements, as done in the OpCode library [43] (and in more recent ones, such as PhysX). An AABB is a set of nested boxes, organized in a binary tree. Each internal node contains two children (each of them having its own bounding box), and in my implementation, each leaf contains a single triangle. Each internal node n , encoded as an integer, knows its two children and its bounding box. The two children are implicitly encoded, by `left_child(n) = 2n` and `right_child(n) = 2n+1` (note that the root node needs to be 1 rather than 0, else the root would be its own left child!). The bounding boxes are simply stored in a contiguous array indexed by n . Now we need to know which triangles correspond to a given node. Again, we store as few information as possible. Instead of storing a set of triangle index in each node, we permute the mesh triangles in such a way that all the triangles corresponding to a given node are contiguous in memory. Hence, the entire mesh, or the sequence of triangle indices $[0, \dots, N_F]$ corresponds to the root node $n = 1$. Then the sequence $[0, \dots, N_F/2]$ corresponds to its left child $n = 2$, and the sequence $[N_F/2, \dots, N_F]$ to its right child, and so on and so forth. Hence node n contains the sequence of triangles $[b, e)$, `left_child(n)` (with index $2 \times n$) contains the sequence $[b, m)$ and `right_child(n)` (with index $2 \times n + 1$) contains the sequence $[m, e)$, with $m = b + (e - b)/2$. With this encoding, instead of being stored, triangle indices are implicitly determined, and propagated through the recursive function calls that traverse the tree.

Such a AABB tree can be easily constructed by first re-ordering the mesh facets, then computing the bounding boxes of each facet, and then recursively create the bounding boxes of higher level

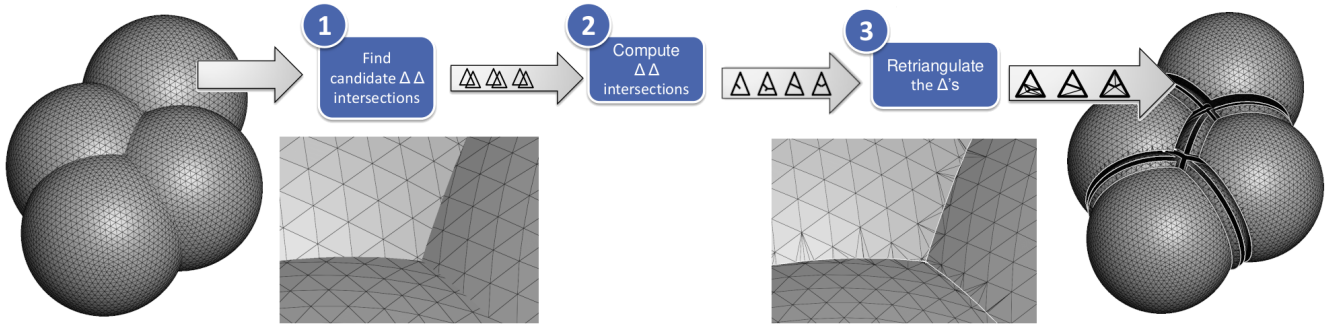


Figure 3: Surface mesh co-refinement takes as input a set of triangulated surface (left). Then, the candidate pairs of intersecting triangles are determined (1), which generates a stream of pairs of triangles. Triangles intersections are computed (2). The result is a stream of triangles with the set of segments that would be inserted into each of them. Finally, a constrained Delaunay triangulation is computed in each triangle (3) and the resulting triangles are merged to create the co-refinement mesh (right, displayed in “exploded view”).

nodes. To re-order the mesh facets, we use balanced Morton ordering (also called balanced Z-curve ordering). It can be easily implemented using the `std::nth_element` function of the Standard Template Library, as done in the spatial sorting package of the CGAL library [6]. The re-ordering of the facets is computed in-place in the mesh data structure. Since we used a balanced AABB-tree, the links in the tree are completely implicit. The only thing that needs to be stored is the array of bounding boxes. Depending on the importance of performance w.r.t. storage requirement, other choices are possible, such as using unbalanced trees constructed with the classical Surface Area heuristic (SAH) [31]. Unbalanced trees require storing for each node the number of triangles in one of the subtrees. On the other end of the spectrum, zero-byte AABBs [43, 44], do not need any additional data structure. They are based on the observation that the bounds of bounding box are coordinates of some vertices in the mesh. At the expense of a small number of additional tests, this makes it possible to encode the entire acceleration structure within the ordering of the triangles and their vertices. In our context, balanced AABBs realize a good compromise between speed and storage.

Now, given a AABB tree that contains all the facets to be intersected, we need to write a function that will determine a superset of all pairs of facets that have an intersection. This superset will correspond to the pairs of facets which bounding boxes have an intersection. It is based on a recursive AABB tree traversal, that determines all the intersections between all bounding boxes in two subtrees planted at nodes n_1 and n_2 respectively. Node n_1 corresponds to the facets sequence $[b_1, e_1)$ and node n_2 to facets sequence $[b_2, e_2)$. The function also takes as an argument a function `DO_IT`, that will be called for each candidate facet pair:

input:

- n_1, b_1, e_1 : first node (n_1) and associated facet sequence $[b_1, e_1)$
- n_2, b_2, e_2 : second node (n_2) and facet sequence $[b_2, e_2)$
- `DO_IT` : function to be called for candidate intersecting facets

```

(1) intersect( $n_1, b_1, e_1, n_2, b_2, e_2, DO\_IT$ )
(2)   if  $e_2 \leq b_1$  then return
(3)   if  $bbox[n_1] \cap bbox[n_2] = \emptyset$  then return
(4)    $N_1 \leftarrow e_1 - b_1$  ;  $N_2 \leftarrow e_2 - b_2$ 
(5)   if  $N_1 = 1$  and  $N_2 = 1$  then DO_IT( $b_1, b_2$ )
(6)   if  $N_2 > N_1$  then
(7)      $m_2 \leftarrow b_2 + N_2/2$ 
(8)     intersect( $n_1, b_1, e_1, left\_child(n_2), b_2, m_2$ )
(9)     intersect( $n_1, b_1, e_1, right\_child(n_2), m_2, e_2$ )
(10)  else
(11)     $m_1 \leftarrow b_1 + N_1/2$ 
(12)    intersect(left_child( $n_1$ ),  $b_1, m_1, n_2, b_2, e_2$ )
(13)    intersect(right_child( $n_1$ ),  $m_1, e_1, n_2, b_2, e_2$ )
(14)  end
(15) end

```

Algorithmic details:

- Line (2) exits the function if the facet sequence corresponding to n_2 is “to the left” of the one corresponding to n_1 . This avoids doing the same traversals twice (once with n_1, n_2 and once with n_2, n_1);
- Line (3) early exits the function if the two bounding boxes of n_1 and n_2 are non-overlapping. It is where the acceleration occurs;
- Line (4) computes the number of facets N_1 in n_1 and N_2 in n_2 ;
- Line (5) handles leaf-leaf intersections, by calling DO_IT;
- Lines (7)–(14) recursively compute intersections by traversing the children of the node that has the largest number of triangles.

At the top level, recursion is launched by calling `intersect(1, 0, N_F , 1, 0, N_F)` where 1 corresponds to the root node of the AABB, and where N_F denotes the number of facets in the mesh.

2.1.2 Computing the intersection between two triangles. The output of the previous step of the algorithm is a stream of potentially intersecting triangle pairs (t, t') , generated by the calls to the `DO_IT(t, t')` function. Now we need to determine within these candidates the ones that correspond to actual intersections. In addition, we need also to determine the coordinates of the intersection points. At first sight, computing the intersection between two triangles is a rather simple task. Whether two triangles overlap can be *exactly* determined using the `orient_3d()` predicate [7]. But in our case, we need more information. We need not only the coordinates of the intersection, but also the associated combinatorial information. Moreover, there is a (surprisingly) large number of possible configurations for the intersection of two triangles. Figure 4-A shows the generic case, where the intersection between the two triangles is a line segment. Each extremity of this line segment correspond to the intersection between one of the triangle’s edges with the supporting plane of the other triangle. However, there are many possible degeneracies, such as a point of one triangle that falls exactly on the other one (B), or two edges that partially overlap (C). If the triangles are coplanar, the intersection can even be a polygon (D) with up to 6 vertices (E)!

To tackle this problem, we will write a function that computes a *combinatorial* representation of the intersection. Each triangle t (resp. t') can be seen as a simplicial set Σ_t with 7 simplices: each triangle has three vertices V_1, V_2, V_3 , three edges $E_1 = (P_2, P_3)$, $E_2 = (P_3, P_1)$, $E_3 = (P_1, P_2)$, and the whole triangle $T = (P_1, P_2, P_3)$. We consider that each simplex is embedded as an open set. In other words, each edge is embedded as a segment minus the extremities, and T is embedded as the triangle minus its border, hence each point of the triangle is contained by exactly one simplex. For each intersection point (in red in Figure 4) we will output the unique pair of simplices σ, σ' whose embeddings contain the point, where $\sigma \in \Sigma_t = \{P_1, P_2, P_3, E_1, E_2, E_3, T\}$ and $\sigma' \in \Sigma_{t'} = \{P'_1, P'_2, P'_3, E'_1, E'_2, E'_3, T'\}$. In practice, in an implementation, the simplices can be encoded as integers, or enums. From this description, one can imagine the following (generic, naive) triangle-triangle intersection algorithm, that tests all the 7×7 possible intersections between the simplices of t and t' :

```
triangle_triangle_naive()
input: two triangles  $t$  and  $t'$ 
output: a list  $I$  of simplices pairs  $(\sigma, \sigma')$ 
         that define the intersection points
```

- (1) **for** σ **in** Σ_t
- (2) **for** σ' **in** $\Sigma_{t'}$
- (3) **if** $\sigma \cap \sigma'$ is a point **then**
- (4) $I \leftarrow I \cup \{(\sigma, \sigma')\}$
- (5) **end**
- (6) **end**
- (7) **end**
- (8) **return** I

It is possible to be much smarter than what is done in the algorithm above. For instance, the triangle-triangle intersection test in [7] determines whether two triangles have an intersection, and minimizes the number of `orient3d` invocations. In our case, we cannot use it directly, because our situation is slightly more complicated: we also need to compute the combinatorial representation of the intersection. But we can avoid some unnecessary tests as follows:

```
triangle_triangle()
input: two triangles  $t$  and  $t'$ 
output: a list  $I$  of simplices pairs  $(\sigma, \sigma')$ 
         that define the intersection points
```

- (1) **if** P_1, P_2, P_3 are strictly on the same side
of the support plane of (P'_1, P'_2, P'_3) **then return** \emptyset
- (2) **for** E **in** $\{E_1, E_2, E_3\}$
- (3) $I \leftarrow I \cup \text{edge_triangle}(E, T')$
- (4) **end**
- (5) **for** E' **in** $\{E'_1, E'_2, E'_3\}$
- (6) $I \leftarrow I \cup \text{edge_triangle}(E', T)$
- (7) **end**
- (8) **return** I

The idea is to have an early-exit test (line 1), then test the three edge of each triangle against the other one. The underlying edge-triangle intersection algorithm works as follows:

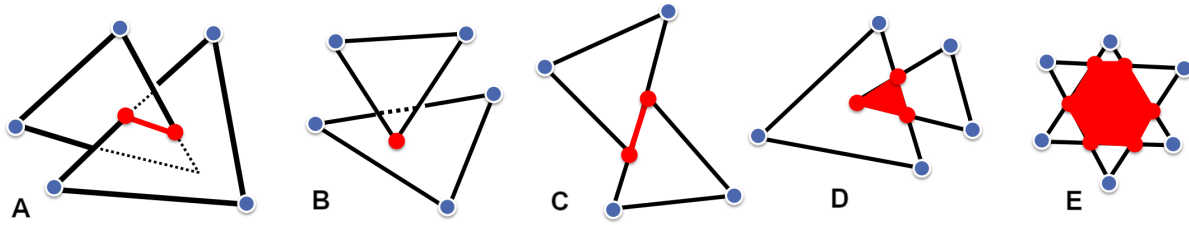


Figure 4: Intersection between two triangles, a surprisingly delicate problem. Some of the configurations one may encounter. There are many other ones !

edge_triangle()

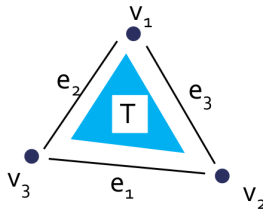
input: an edge E and a triangle T

output: a list I of simplices pairs (σ, σ') that define the intersection points

-
- (1) $(P_1, P_2, P_3) \leftarrow \text{vertices}(T)$
 - (2) $(Q_1, Q_2) \leftarrow \text{vertices}(E)$
 - (3) $s_1 \leftarrow \text{orient3d}(P_1, P_2, P_3, Q_1)$
 - (4) $s_2 \leftarrow \text{orient3d}(P_1, P_2, P_3, Q_2)$
 - (5) **if** $s_1 \times s_2 > 0$ **then return** \emptyset
 - (6) **if** $s_1 = 0$ **and** $s_2 = 0$ **then return** edge_triangle_2D(E, T)
 - (7) $o_1 \leftarrow \text{orient3d}(Q_1, Q_2, P_1, P_2)$
 - (8) $o_2 \leftarrow \text{orient3d}(Q_1, Q_2, P_2, P_3)$
 - (9) $o_3 \leftarrow \text{orient3d}(Q_1, Q_2, P_3, P_1)$
 - (10) **if** $o_1 \times o_2 < 0$ **or** $o_2 \times o_3 < 0$ **or** $o_3 \times o_1 < 0$ **then return** \emptyset
 - (11) $R_1 \leftarrow \text{region}(T, o_1, o_2, o_3)$
 - (12) $R_2 \leftarrow \text{region}(E, s_1, s_2)$
 - (13) **return** (R_2, R_1)

Algorithmic details:

- Line (5): if both extremities of E are on the same side of T then there is no intersection;



$$\Sigma_t = \{ v_1, v_2, v_3, e_1, e_2, e_3, T \}$$

Figure 5: A triangle t seen as a simplicial set Σ_t , decomposed into 7 open regions: its three vertices v_1, v_2, v_3 , the three edges e_1, e_2, e_3 (minus their extremities) and the “meat” of the triangle T (minus the border). This (trivial) way of considering a triangle makes it easy to design a correct algorithm that determines the combinatorial intersection between two triangles that works for all possible degenerate cases (some of them depicted in Fig. 4 above).

- Line (6): if both extremities of E are on the supporting plane of T then we are in 2D and it is a special case, using a different codepath (more on this later);
- Line (10): if two of o_1, o_2, o_3 have opposite sign, then the intersection between E and the supporting plane of T is outside T ;
- Line (11): if exactly one of o_1, o_2, o_3 is 0, then the intersection is on an edge of T . If two of them are 0, then the intersection is on a vertex of T . The function region returns this edge or this vertex or T depending on which of o_1, o_2, o_3 is zero;
- Line (12): same thing with the edge E : if one of s_1, s_2 is zero, then the intersection is on a vertex of E ;

The function edge_triangle_2D() will not be detailed explicitly here⁴, but we give an idea of how it works. It first finds a direction of projection, then determines whether, in 2D, E 's extremities are in T , then computes the intersection between E and the three edges of the triangle in 2D. For edges that are co-linear (like in Figure 4-C), there is a edge_triangle_1D() function that determines the intersection by comparing intervals.

The number of invocations to the orient_3d predicate remains higher than the optimal, because our algorithm naively computes intersection between sub-simplices without taking into account more global information. To avoid doing the same computations several times, we use a “predicate cache”, indexed by the sorted list of its four arguments, and changing the sign in function of the parity of the actual order of the four arguments (orient_3d is a determinant, hence permutting its columns changes the sign depending on the parity of the permutation).

The output of the algorithm is a list I of couples (σ, σ') that correspond to all intersection points (red dots in Figure 4). Each simplex σ, σ' can be encoded as an integer in $[0, \dots, 6]$. Note that since we divided the initial problem (triangle-triangle intersection) into simpler independent problems (edge-triangle, edge-edge intersections), one may obtain the same intersection several times. Duplicated intersections can be eliminated by sorting the list of couples (σ, σ') (using std::sort() with the lexicographic order for instance) and eliminating the duplicates (using std::uniq()).

The method we have described so far is able to handle triangle-triangle intersection when the result is a segment (Figure 4-A and C) or a point (Figure 4-B). When the intersection is a polygon (Figure

⁴but is available in the companion source-code.

4-D and E), the method outputs all the vertices of the polygon, but they come in an arbitrary order, so we need to order them along the boundary of the intersection polygon. In fact, what we need is finding all the edges of the intersection polygon (because they will be positioned as Delaunay constraints, more on this in the next subsection). The idea is to test all possible edges of the intersection polygon, and keep only the ones that are on the boundary of the intersection polygon (red edges in Figure 4 D and E). In other words, given two intersection points, defined by the couples of simplices (σ_1, σ'_1) and (σ_2, σ'_2) , how can we determine if the so-defined edge is on the border of the intersection? One can observe that an edge of the intersection is always a subset of an edge of one of the triangles, hence we just need to test if σ_1 and σ_2 are on the same edge of t or σ'_1 and σ'_2 are on the same edge of t' . This test is very simple, two simplices σ_1 and σ_2 are on the same edge if:

- $\sigma_1 = \sigma_2 = e$ where e is an edge, or
- σ_1 is an edge and σ_2 is a vertex of σ_1 , or
- σ_2 is an edge and σ_1 is a vertex of σ_2

To summarize, once we have determined all the intersection points, there are three cases:

- (1) **there is a single point:** the intersection is degenerate and is a point;
- (2) **there are two points:** the intersection is the segment that connects both points;
- (3) **there are more than two points:** the intersection is a polygon. One obtains its edges by testing all possible couples of points (maximum 15 couples to test). It is a trivial combinatorial test.

At the end of this step, what we obtain is for each triangle t , a list of segments generated from an intersection between t and other triangles. For each segment extremity, we know the couple of simplices σ, σ' that generated the intersection. The next step of the algorithm is to remesh each triangle in such a way that all segments are explicitly represented in the resulting mesh.

2.1.3 Constrained Delaunay Triangulation. We need to insert a list of points and segments in each triangle, hence we need to compute a large number of *constrained* triangulations. These triangulations are computed in 2D. It is possible to use 2D coordinates in the supporting plane of each triangle, however, with the exact number representation that we use, it has the non-negligible cost of nesting additional dot products in the expressions. As often done in other works, I chose instead to peek the two coordinates of the triangle's normal that have the smallest absolute values. As noted in [4], this requires special care: comparing the magnitudes of the components of the normal vector needs to be done in exact arithmetics, else one may project along axes that create degenerate configurations. It can happen for instance with a very skinny triangle with a normal close to $[1, 1, 1]$. Due to floating point rounding error, one may pick a projection axis onto which the triangle degenerates into a segment. Invoking exact arithmetics for finding the dominant axis of a normal vector is not pedantic as one may think: I encountered this problem with mesh #356074 from [52]⁵.

⁵I find it worth it to confess that I learned the lesson the hard way, required some debugging, I should have believed them [4] right from the beginning !

In addition to the triangulation being *constrained*, it is interesting to require it to be a constrained *Delaunay* triangulation for two reasons:

- With Delaunay, the quality of the mesh is “not too bad”, because it maximizes the smallest angle. We say here “not too bad” because in general, even with Delaunay, intersection meshes contain small angles and cannot be directly used in numerical simulation without some re-meshing / post-processing. However, it is always good to have a starting point that does not have too many triangles with very small angles;
- the Delaunay triangulation is unique, which is an interesting property when the intersecting meshes have overlapping coplanar facets. This property ensures that the same zone will be meshed with the same triangles (one only needs to filter-out the duplicated triangles). There exists other method to solve the problem with non-unique triangulations, based on a cavity-remeshing operator with linear complexity [27], but this require maintaining a list of polygons together with the triangulations, and identifying the duplicated polygons, using a more complicated data structure. In other words, this means pushing the difficulties into the combinatorial data structure. We prefer to keep them in the predicates, because predicates are concentrated in a small portion of the code, easier to maintain and to debug.

In our “wish list” for the constrained Delaunay triangulation code, we need the following two properties:

- **genericity:** since the extremities of the constrained edges are intersection points, their coordinates are not represented as standard floating-point, and the algorithm needs to be adapted to these “exotic” points;
- **efficiency:** the new code will be deployed in an industrial context, and needs to have performances that are on par with the standards. In particular, in principle, re-meshing all pairs of intersected triangles can be performed in parallel, so the constrained Delaunay triangulation code needs to be multithread-friendly (no dynamic allocations, as few locks as possible).

There are several implementations of a constrained Delaunay triangulation available, such as Shewchuk's *Triangle* [38] and CGAL [45]. We chose not to use them for several reasons. First, *Triangle* has hardwired predicates (whereas we need to plug special ones, adapted to points that come from intersections), and it has global variables, preventing it to be used in a multithreaded context. CGAL can be completely parameterized through a template mechanism. However, by default, it internally uses pointer-based data structures that do dynamic allocations, which has an impact of performance in a multithreaded context.

There are many references about constrained Delaunay triangulations, but most of them focus on its mathematical properties and few of them focus on how to implement it. A description of a reasonably efficient algorithm that works is given in one of the first references on this topic [40]. There are faster algorithms (divide and conquer, used in [38]), but we will stick to a simple algorithm to keep the implementation simple and easy to maintain. Moreover,

since our coordinates are going to be the result of intersections, execution time will be largely dominated by the predicates, so we can afford slightly suboptimal combinatorics, provided that predicates invocation remains minimal. For that, we use a predicate cache, as in the triangle-triangle intersection routine (§2.1.2 p.7).

Sloan’s algorithm is reasonably easy to implement, because it is (mostly) based on a single geometric operation: flip the edge common to two triangles. Before we dive into the detail, let us see a high-level version of the algorithm:

```

constrained_Delaunay_triangulation
input:
  a triangle  $t_0 = (p_0, p_1, p_2)$ 
  a list of vertices  $p_i, i = 3 \dots N_v$  inside  $t$ 
  a list of edges  $E_k = (i_k, j_k), k = 1 \dots N_e$ 
output:
  the Delaunay triangulation of the  $p_i$ 's
  constrained by the  $E_k$ 's and by  $t$ 's edges.

```

-
- (1) **for** $i = 1$ **to** N_v
 - (2) find the triangle t that contains p_i
 - (3) insert p_i into t
 - (4) push the three triangle edges opposite to p_i onto S
 - (5) Delaunayize_vertex_neighbors(p_i, S)
 - (6) **end**
 - (7) **for** $k = 1$ **to** N_e
 - (8) enqueue the edges intersecting (i_k, j_k) onto Q
 - (9) $N \leftarrow$ constrain_edges(i_k, j_k, Q)
 - (10) Delaunayize_new_edges(N)
 - (11) **end**

The algorithm starts from a single triangle $t_0 = (p_0, p_1, p_2)$ and inserts the vertices and the edges into it one by one. It is made of two main blocks:

The first block. (lines (1) to (6)) inserts the vertices one by one in the triangulation, by first locating the triangle t that contains the point p_i . Then it splits this triangle into three (note that p_i can be exactly located on an edge, then the two triangles that share that edge are split into two, for a total of four new triangles). Then the Delaunay condition is restored by the Delaunayize_vertex_neighbors() function. This function recursively flips the edges that violate the Delaunay condition and pushes the new triangle on the stack S until the stack is empty. The reader is referred to the original article [40] for more details.

The second block. (lines (7) to (11)) inserts the constraints one by one in the triangulation. The first step (line (8)) detects the edges that have an intersection with the constraint. This is done by “walking the triangulation” along the edge, one triangle at a time, and testing for each triangle two edges (the third one is the one we came from). If one of the intersected edge is a constraint, then this means we have detected a triple point, like in Figure 1-C, where the intersection of edges e_1 and e_2 generate a new vertex I . The intersected edges are pushed to a queue Q . Then the function constrain_edges() processes each “flippable” edge of the queue until the queue is empty. By “flippable”, we mean that the two

triangles adjacent to the edge form a convex polygon. It can be proven that this process converges. Each time an edge is flipped, the corresponding triangles are saved in a list N of “new” triangles, finally processed by the Delaunayize_new_edges() function that flips edges until the Delaunay condition is satisfied everywhere.

My implementation is classical and follows this framework, with a couple of adaptations:

- (1) first, we are going to compute a huge number of constrained Delaunay triangulations, in each individual triangle that has intersections. To keep performance acceptable, we are going to construct them in parallel. Dynamic memory allocation is a serious obstacle to efficient parallel code, because there is a global lock associated with the malloc() function (or the new() operator), so our data structure will be solely composed of std::vector’s allocated once for all⁶. We also need a data structure for the stack of triangles S and the queue of triangles Q . We use a doubly connected list, represented as two additional std::vector’s that store the forward and backward link;
- (2) second, the algorithm manipulates edges. To keep things simpler, we systematically designate an edge through a triangle, and rotate the triangle in place in such a way that the designated edge is edge 0.

The algorithm to restore de Delaunay condition around new vertices and around new edges is as in the classical implementations of the Bowyer-Watson algorithm. The algorithm to constrain the edges deserves more details, because the way the edges are systematically manipulated through triangles reveals an optimization that avoids most invocations to the orient_2d predicate. The classical version is as follows:

⁶except at the beginning when they will grow as needed, and later, they never shrink.

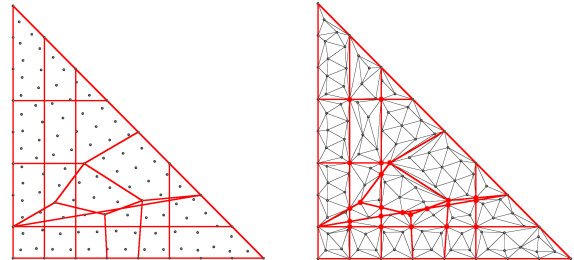


Figure 6: Constrained Delaunay Triangulation in 2D. Left: input points and constraints. Note that some constraints have intersections. Right: the resulting triangulation. The vertices that correspond to constraint intersections were automatically inserted.

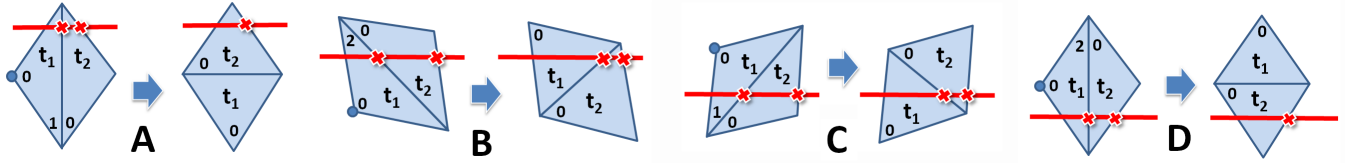


Figure 7: The four configurations of triangle flips that can be encountered during the constraint enforcement phase. The constrained edge (i, j) is shown in red. The four configurations are determined by (1) the orientation of $t_1.v_0$, shown as a (pale) blue dot, with respect to (i, j) and (2) whether $t_2.v_0$ corresponds to $t_1.v_1$ or $t_1.v_2$. By exploiting the combinatorial information, one tests whether a triangle's edge intersects the constraint (i, j) with a single `orient_2d` invocation (instead of up to 4)

`constrain_edges`

input:

the edge i, j to be constrained

a queue Q initialized with the edges intersected by (i, j)

output:

the set N of new edges

```

(1)  while  $Q$  is not empty
(2)     $(v_1, v_2) \leftarrow \text{dequeue}(Q)$ 
(3)    if the two triangles incident to  $(v_1, v_2)$  form a convex quad
(4)      swap_edge( $v_1, v_2$ )
(5)      if  $(v_1, v_2) \cap (i, j) \neq \emptyset$  then
(6)        enqueue( $Q, (i, j)$ )
(7)      else
(8)         $N \leftarrow N \cup (v_1, v_2)$ 
(9)      end
(10)   else
(11)     enqueue( $Q, (i, j)$ )
(12)   end
(13) end

```

The segment-segment intersection test in line (5) that normally requires up to 4 invocations of the `orient_2d` predicate can be replaced with a single invocation and some combinatorics. Remember that each edge (v_1, v_2) is systematically manipulated through a triangle (v_0, v_1, v_2) , rotated in such a way that its vertex v_0 is opposite to the edge under consideration. Then, as shown in Figure 7, there are four different configurations for the pair of triangles $t_1 = (v_0, v_1, v_2)$ and t_2 adjacent to t_1 along (v_1, v_2) , depending on whether t_2 is in the queue Q of intersected edges⁷, depending on `orient_2d`(i, j, v_0) and depending on whether t_2 's first vertex is v_1 or v_2 :

- $t_2 \notin Q$ then after swapping there can't be any intersection then (v_1, v_2) is pushed to N (new edge);
- config. A: `orient_2d`(v_0, i, j) < 0 and $t_2.v_0 = t_1.v_1$ then t_1 is pushed to N (new edge);
- config. B: `orient_2d`(v_0, i, j) < 0 and $t_2.v_0 = t_1.v_2$ then t_1 is pushed to Q (still has an intersection);
- config. C: `orient_2d`(v_0, i, j) > 0 and $t_2.v_0 = t_1.v_1$ then t_1 is pushed to Q (still has an intersection);
- config. D: `orient_2d`(v_0, i, j) > 0 and $t_2.v_0 = t_1.v_2$ then t_1 is pushed to N (new edge)

⁷that is tested in $O(1)$ using a per-triangle array of marks.

I give also here a short comment on another part of the algorithm, that determines the list of edges intersected by the constraint (i, j) . This part of the algorithm is conceptually simple (just walk along the triangles according to `orient_2d`), very similarly to what is done for locating a point), but there are three subtleties:

- whenever an existing vertex v lands exactly on the constrained edge (i, j) , one needs to traverse the fan of triangles incident to v in order to find the next triangle;
- there can be co-linear overlapping constraints, hence one needs to store in each segment the list of constraints it belongs to. In my implementation they are chained. This information is required for instance when classifying the triangles;
- whenever an intersecting edge is also a constraint, one needs to insert the intersection of both constraints into the triangulation, and delaunay-ize its neighborhood, before enforcing the edge constraints.

An example of a 2D constrained Delaunay triangulation with intersecting constraints is shown in Figure 6. The constrained segments are shown in red. Some of them have intersections (red dots). The algorithm automatically detects the intersections, inserts them in the triangulation, respects all the constraints and the Delaunay criterion.

Let us see now how the geometric part of the algorithm works. First, one can notice that the constrained Delaunay triangulation is mostly combinatorial. The only places where geometrical information is used is a set of three functions. The first two ones are *predicates*, that return a sign (negative, zero or positive):

- `orient`(i, j, k): computes the 2D orientation of the triangle with vertices i, j and k . It is used in many places, to detect the triangle that contains an inserted point, to test for intersecting edges, and to test whether an edge is flippable.
- `incircle`(i, j, k, l): this corresponds to the Delaunay condition (the circumscribed circle of each triangle should not contain any vertex). This function is symbolically perturbed, in such a way that it never returns zero (see [10]). This ensures a unique triangulation for configurations with cocyclic vertices.

The third function is a *construction*, that creates new geometry:

- `create_intersection`(i, j, k, l): create a new vertex that corresponds to the intersection between edges (i, j) and (k, l)

So now the question is how to implement these three functions given that some of our vertices are given as intersections between segments and triangles. The strategy here is to keep the algorithm as near as possible to “simply implement the math”. In other words, it means we are pushing most of the difficulties towards the geometric kernel (predicates and constructions) to keep the overall structure of the algorithm simple (nearly a verbatim copy of the textbook algorithm). So we are going to compute the coordinates of the intersection points explicitly. Since these coordinates are rational fractions, and since computations for x, y and z are inter-related, it is reasonable to represent the intersection points in homogeneous coordinates $\hat{\mathbf{p}} = [x \ y \ z \ w]$ that corresponds to a 3D point $\mathbf{p} = [x/w \ y/w \ z/w]$. Each individual x, y, z, w coordinate is represented in an *exact number type* that exactly implements addition, subtraction and multiplication. We shall see later (§2.4 p.17) two alternatives to implement exact number types, and how to implement all the predicates that we need.

The input of the constrained Delaunay triangulation is a triangle t_1 and the list of segments to be inserted into t_1 . Each segment’s extremity is encoded symbolically, as a triple σ_1, t_2, σ_2 , indicating the location of the intersection within t_1 , the other facet t_2 and the location of the intersection within t_2 . Note that there can be also individual points (for instance, when a vertex is exactly located in a facet). The first task to do is computing the coordinates of each intersection. Depending on the nature of σ_1 and σ_2 , there are three different cases, plus an additional case for intersecting constraints:

- initial vertex: just convert the input point (with floating-point coordinate) to the arbitrary precision representation;
- edge $e_1 \cap$ triangle t_2 in 3D or edge $e_1 \cap$ edge e_2 in 3D;
- edge \cap edge in 2D;
- intersection of two constraints

Let us detail now how to compute the coordinates of the intersection point \mathbf{I} for the last three configurations:

edge $e_1 \cap$ triangle t_2 in 3D or edge $e_1 \cap$ edge e_2 in 3D: Let \mathbf{q}_1 and \mathbf{q}_2 denote the extremities of the edge and let $\mathbf{p}_1, \mathbf{p}_2$ and \mathbf{p}_3 denote the vertices of the triangle. We are in 3D if \mathbf{q}_1 and \mathbf{q}_2 are not both in the supporting plane of $\mathbf{p}_1, \mathbf{p}_2, \mathbf{p}_3$ (in other words, at least one of $\text{orient_3d}(\mathbf{p}_1, \mathbf{p}_2, \mathbf{p}_3, \mathbf{q}_1)$ and $\text{orient_3d}(\mathbf{p}_1, \mathbf{p}_2, \mathbf{p}_3, \mathbf{q}_2)$ is non-zero). Note that if we are in 3D, the *edge $e_1 \cap$ edge e_2* configuration can be seen as a particular case of the *edge $e_1 \cap$ triangle t_2* case, by replacing e_2 by the triangle t_2 it comes from. At the previous step, we already determined that the intersection exists, so to compute its coordinate we just need to compute a line-plane intersection, without needing to check that the intersection is in the segment and in the triangle. The intersection point \mathbf{I} belongs to the line:

$$\mathbf{I} = \mathbf{q}_1 + t(\mathbf{q}_2 - \mathbf{q}_1) \quad t \in \mathbb{R}$$

and to the plane:

$$(\mathbf{I} - \mathbf{p}_1) \cdot \mathbf{N} = 0 \quad \text{where } \mathbf{N} = (\mathbf{p}_2 - \mathbf{p}_1) \times (\mathbf{p}_3 - \mathbf{p}_1).$$

By substituting, one gets:

$$t = \frac{(\mathbf{p}_1 - \mathbf{q}_1) \cdot \mathbf{N}}{(\mathbf{q}_2 - \mathbf{q}_1) \cdot \mathbf{N}} \quad ; \quad \mathbf{I} = \text{mix}(t, \mathbf{q}_1, \mathbf{q}_2)$$

$$\text{where } \text{mix}(t, \mathbf{q}_1, \mathbf{q}_2, t) = \mathbf{q}_1 + t(\mathbf{q}_2 - \mathbf{q}_1) = (1 - t)\mathbf{q}_1 + t\mathbf{q}_2.$$

One needs to keep in mind that these computations are made with exact numbers (more on this in (§2.4 p.17)). Since our exact numbers only support addition, subtraction and product, and since t is a rational number, the intersection \mathbf{I} will be represented in homogeneous coordinates. So we need an implementation of $\text{mix}(t, \mathbf{q}_1, \mathbf{q}_2)$ that takes two points $\mathbf{q}_1, \mathbf{q}_2$ with floating-point coordinates, an exact rational parameter t , and that returns a point with homogeneous coordinates:

$$\text{mix}\left(\frac{a}{b}, \mathbf{q}_1, \mathbf{q}_2\right) = \frac{a}{b}\mathbf{q}_2 + \frac{b-a}{b}\mathbf{q}_1 = \left[\begin{array}{c} a\mathbf{q}_2 + (b-a)\mathbf{q}_1 \\ b \end{array} \right]_h$$

where the h subscript indicates that the point has homogeneous coordinates. Note that one could also use 3d vectors with the x, y, z coordinates as independent rational numbers instead of homogeneous coordinates.

edge \cap edge in 2D: computing the intersection of two coplanar edges cannot be done by the formula above (because for coplanar edge and triangle, the denominator is zero), so we compute the intersection in 2D (using the 2×2 Cramer formula), and lift it to 3D using the 3D points P_1 and P_2 associated with p_1 and p_2 :

$$\begin{aligned} \mathbf{I} &= \text{mix}(t, \mathbf{p}_1, \mathbf{p}_2) \quad \text{where:} \\ t &= \det(\mathbf{q}'_1 - \mathbf{p}'_1, \mathbf{q}'_2 - \mathbf{q}'_1) / \det(\mathbf{p}'_2 - \mathbf{p}'_1, \mathbf{q}'_2 - \mathbf{q}'_1), \end{aligned}$$

and where $\mathbf{p}_1, \mathbf{p}_2, \mathbf{q}_1, \mathbf{q}_2$ denote the (3D) extremities of the two segments, and $\mathbf{p}'_1, \mathbf{p}'_2, \mathbf{q}'_1, \mathbf{q}'_2$ denote the (2D) projected extremities of the two segments.

intersection of two constraints: the last possible configuration for a constructed intersection point is encountered whenever two constrained segments have an intersection (see Figure 1). Clearly, it is possible to reuse the 2D segment intersection formula above, and lifting it to 3D (by t -mixing the 3D points instead of the 2D points). However, the resulting expression has two nested levels of exact operations (expression of t and $\text{mix}()$). It especially has an impact on performance when using the arithmetic expansions (§2.4.1 p.17). By recalling that an intersection between two constraints systematically corresponds to an intersection between three triangles, one can obtain a simpler and more symmetric equation for the intersection. The intersection between three triangles can be obtained easily, using the 3×3 Cramer formula:

$$\left[\begin{array}{ccc} a_{11} & a_{12} & a_{13} \\ a_{21} & a_{22} & a_{23} \\ a_{31} & a_{32} & a_{33} \end{array} \right] \left[\begin{array}{c} x_1 \\ x_2 \\ x_3 \end{array} \right] = \left[\begin{array}{c} y_1 \\ y_2 \\ y_3 \end{array} \right] \Rightarrow$$

$$x_1 = \frac{\left| \begin{array}{cc} y_1 & a_{12} & a_{13} \\ y_2 & a_{22} & a_{23} \\ y_3 & a_{32} & a_{33} \end{array} \right|}{\left| \begin{array}{ccc} a_{11} & a_{12} & a_{13} \\ a_{21} & a_{22} & a_{23} \\ a_{31} & a_{32} & a_{33} \end{array} \right|}$$

$$x_2 = \frac{\left| \begin{array}{cc} a_{11} & y_1 & a_{13} \\ a_{21} & y_2 & a_{23} \\ a_{31} & y_3 & a_{33} \end{array} \right|}{\left| \begin{array}{ccc} a_{11} & a_{12} & a_{13} \\ a_{21} & a_{22} & a_{23} \\ a_{31} & a_{32} & a_{33} \end{array} \right|}$$

$$x_3 = \frac{\left| \begin{array}{cc} a_{11} & a_{12} & y_1 \\ a_{21} & a_{22} & y_2 \\ a_{31} & a_{32} & y_3 \end{array} \right|}{\left| \begin{array}{ccc} a_{11} & a_{12} & a_{13} \\ a_{21} & a_{22} & a_{23} \\ a_{31} & a_{32} & a_{33} \end{array} \right|}$$

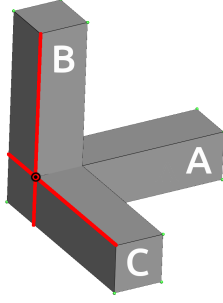


Figure 8: The intersection between two edges of B and C (in red) landing exactly on a corner of A (highlighted).

Given our three triangles (p_1, p_2, p_3) , (q_1, q_2, q_3) and (r_1, r_2, r_3) , the intersection I is given by:

$$I = \left[\begin{array}{c} \left[\begin{array}{ccc|c} B_x & N_{1y} & N_{1z} & \\ B_y & N_{2y} & N_{2z} & \\ B_z & N_{3y} & N_{3z} & \end{array} \right] \\ \left[\begin{array}{ccc|c} N_{1x} & B_x & N_{1z} & \\ N_{2x} & B_y & N_{2z} & \\ N_{3x} & B_z & N_{3z} & \end{array} \right] \\ \left[\begin{array}{ccc|c} N_{1x} & N_{1y} & B_x & \\ N_{2x} & N_{2y} & B_y & \\ N_{3x} & N_{3y} & B_z & \end{array} \right] \\ \left[\begin{array}{ccc|c} N_{1x} & N_{1y} & N_{1z} & \\ N_{2x} & N_{2y} & N_{2z} & \\ N_{3x} & N_{3y} & N_{3z} & \end{array} \right]_h \end{array} \right]$$

where N_1, N_2, N_3 denote the normal vectors of the three triangles, and where $B = [N_1 \cdot p_1, N_2 \cdot q_1, N_3 \cdot r_1]$. As in the previous case, one does not need to check whether the intersection of the supporting planes belongs to the triangles. We already know it does because it is the triangle-triangle intersection function that generated the constraints.

At this point, we are able to generate the coordinates of the constructed points for the three possible configurations for an intersection (edge-triangle or edge-edge in 3D, edge-edge in 2D, and three triangles). The combinatorial part of the constrained Delaunay triangulation queries the geometry through the classical `orient2d` and `incircle` predicates. We shall see later how to implement them, as well as the other ones used by the subsequent steps of the algorithm (§2.4 p.17).

The global vertex table. We have computed the exact coordinates of the intersection points, and we have inserted all the intersection segments into the triangles. Consider an intersection I between a triangle t and an edge e shared by two triangles t_1 and t_2 . The intersection I will be generated twice (once when triangulating t_1 and once when triangulating t_2). Clearly, one could use a key made of integer ids that define e and t to index a global vertex table. However, some nasty configurations may appear. There are two cases:

- two different intersections may land exactly on the same point;
- an intersection may land exactly on a vertex that exists in the input meshes.

Again, considering these cases is not academic paranoia taking the exact computation paradigm too seriously, they often occur in practice. Figure 8 shows one of the simplest example, with three intersecting rods forming a corner. The point in red is the intersection between the two highlighted edges of rods B and C. It exactly corresponds to a vertex of A. This type of configuration is very likely to appear in CAD objects generated by CSG.

In the exact geometry paradigm, in a certain sense, “geometry is combinatorics”, hence, to handle all these configuration, the idea is to use a global vertex table indexed by the coordinates of the points. Implementing a table (e.g., with `std::map` from the C++ STL) requires a function to compare two keys (two points in our case), so we are going to use the lexicographic order on the point’s coordinates. However, one needs to remember that the representation of a point in homogeneous coordinates is non-unique, hence one cannot simply use the lexicographic order on x, y, z, w . Instead of that, we compare the (rational) Euclidean coordinates of the points $x/w, y/w, z/w$, which can be done as follows with our exact number type that does not have division:

$$\text{sign} \left(\frac{x_1}{w_1} - \frac{x_2}{w_2} \right) = \text{sign}(w_1) \times \text{sign}(w_2) \times \text{sign}(w_2 x_1 - w_1 x_2)$$

We shall see (§2.4 p.17) some optimizations that can be made depending on the used exact arithmetic kernel.

To keep the size of the table reasonable, the vertices of the input meshes are not inserted into the table: they are instead processed “the other way round”, at the end of the algorithm, a post-processing phase queries the table with all the input point and merges the co-located ones.

2.2 Mesh boolean operations and CSG

2.2.1 The Weiler model. To evaluate boolean expressions, we construct a combinatorial representation of the relations within a volumetric mesh, called the Weiler model [49]. In what follows, I shall use the notations of combinatorial maps [25].

A 3-dimensional combinatorial map (3-map) is defined as a quadruple $(\mathcal{D}, \sigma_1, \alpha_2, \alpha_3)$, where \mathcal{D} is a set of N discrete elements called *darts*, symbolized as black arrows in Figure 9, that can be identified with the integers $[1..N]$. The three functions $\sigma_1, \alpha_2, \alpha_3$, acting on the set of darts \mathcal{D} , are defined as follows:

- σ_1 is a permutation, that maps each dart to its successor around a triangle;
- α_2 is an involution ($\alpha_2 \circ \alpha_2 = \text{Id}$), that maps each dart to the opposite dart in the neighboring triangle within the same surface (double green lines in Figure 9);
- α_3 is an involution that maps each dart to the opposite dart within the adjacent surface sheet (triple red lines in Figure 9).

As can be seen, each triangle is composed of three darts. In practice, only triangles and α_2, α_3 are stored explicitly. A triangle with index t corresponds to three darts $3t, 3t + 1, 3t + 2$, and the involution σ_1 is given by $\sigma_1 = d - (d \bmod 3) + (d + 1) \bmod 3$.

It is worth mentioning that α_2 and α_3 systematically connect darts with opposite orientations. As a consequence, non-orientable

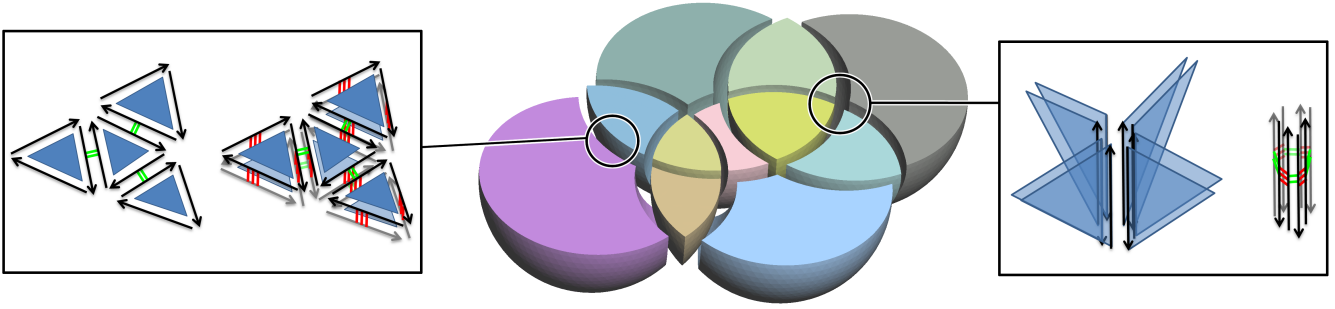


Figure 9: Weiler model and 3-Maps. A 3-map is composed of a set of darts (black arrows), a permutation σ_1 that connects each dart to its successor around a triangle, an involution α_2 (double green lines) that connects each dart to the opposite dart in a neighboring triangle and an involution α_3 (triple red lines) that connects each dart to the opposite dart in the twin sheet. Non-manifold edges form bundles of more than four darts, and need a geometric radial sort.

surfaces (Moebius strip, klein bottle ...) cannot be represented with a 3-map. For the interested reader, there exists a notion of generalized map [26] that represents a wider class of objects (cellular quasi-manifold), comprising non-orientable surfaces. In our context, since we compute CSG and boolean operations, the surfaces we consider are supposed to define closed volumes, hence they are orientable.

One can also define the *orbit* $\langle \beta_1, \beta_2, \dots, \beta_n \rangle (d)$ as the set of darts that can be recursively reached by traversing all links $\beta_1, \beta_2, \dots, \beta_n$ from a dart d . There are 8 possible types of orbits, the following ones are of particular interest:

- **individual triangle:** $\langle \sigma_1 \rangle (d)$
- **shell:** $\langle \sigma_1, \alpha_2 \rangle (d)$, that is, the boundary of one of the colored volumetric regions in Figure 9;
- **bundle:** $\langle \alpha_2, \alpha_3 \rangle (d)$, that correspond to the fan of triangles incident to the same edge. A bundle is non-manifold if it has more than four darts (Figure 9-right). Bundles are referred to as “radial edges” in Weiler’s parlance;
- **connected component:** $\langle \sigma_1, \alpha_2, \alpha_3 \rangle (d)$.

In addition, we define a notion of patch. The patch incident to a dart d is defined by $\langle \sigma_1, \bar{\alpha}_2 \rangle (d)$, where $\bar{\alpha}_2 \rangle (d)$ is defined by:

$$\begin{aligned} \bar{\alpha}_2(d) &= \alpha_2(d) \text{ if the bundle incident to } d \text{ has 4 darts} \\ \bar{\alpha}_2(d) &= d \text{ otherwise.} \end{aligned}$$

Note that the zone where two shells are in contact corresponds to two different charts, one for each side.

2.2.2 Constructing the Weiler model. Now our goal is to construct the Weiler model from the output of the co-refinement phase. We start by duplicating all the triangles, and connecting each dart to its counterpart with α_3 links. Then we identify the bundles by sorting all the darts in lexicographic order based on the indices of their two extremities. In the sorted list of darts, the bundles are easy to find as contiguous sequences with the same extremities. For each bundle, they are two cases to consider:

- **the bundle has 4 darts:** this is the easy case, that corresponds to a manifold edges. We just need to create two α_2 links connecting each part of darts;

- **the bundle has more than 4 darts:** the bundle corresponds to a non-manifold edge (like in Figure 9-right). To determine which darts should be connected with α_2 links, one needs to (geometrically) sort the triangles around the non-manifold edge, an operation referred to as *radial sort* in [49].

To define a total order of the darts around a halfedge, one picks one of the darts h_0 as the origin, and one uses two predicates:

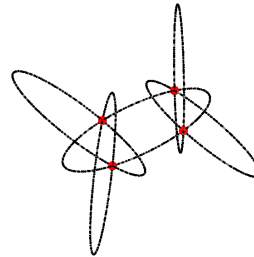
- $\text{orient}(h_1, h_2) = \text{orient_3d}(p_1, p_2, p_3, p_4)$ where p_1 and p_2 are the two extremities of the radial edge and p_3 and p_4 the two vertices opposite to the radial edge in the two triangles incident to h_1 and h_2 ;
- $\text{Norient}(h_1, h_2) = \text{sign}(\mathbf{n}_1 \cdot \mathbf{n}_2)$ where \mathbf{n}_1 and \mathbf{n}_2 denote the normals to the triangles incident to h_1 and h_2 .

For a given dart h in the bundle, the two signs given by $\text{orient}(h_0, h)$ and $\text{Norient}(h_0, h)$ determine four quadrants around the radial edge. If the two darts h_1, h_2 to be compared are in a different quadrant, then their relative order is known. If h_1, h_2 are in the same quadrant, then their relative order is determined by $\text{orient}(h_1, h_2)$.

As for the predicates used in the other stages of the pipeline, these two predicates are filtered using interval arithmetics. The vector $p_2 - p_1$ of the radial edge and the normal vector \mathbf{n}_0 are computed at the beginning of radial sort, in both interval and exact arithmetic.

Note that in these predicates, the two points p_1 and p_2 along the radial edge are intersection points, hence they are represented with homogeneous exact coordinates. As a consequence, even with the interval filters, sorting all the radial edges takes a significant amount of time. However, one can gain significant performance by noticing that the order around a radial edge remains the same

when traversing polygonal lines incident to the same set of patches. Hence one can propagate the order along radial polylines, stopping



at the vertices incident to more than two bundles, shown in red in the small figure.

Once all the radial edges are sorted, the combinatorial links σ_0 , α_2 and α_3 can be set:

- The links σ_0 (that connect each dart to its successor around the triangle) and α_3 (that connect each part of triangles adjacent to the same chart) are trivial to obtain (they do not depend on the radial sort);
- around each bundle $d_1, d_2 \dots d_k$, an α_2 connection is created between each pair of darts $\alpha_3(d_i)$ and $d_{i \oplus 1}$, where $i \oplus 1$ denotes $i + 1$ modulo k .

2.2.3 Classifying. Once the Weiler model is constructed, the next step consists in *classifying* the triangles (step 3 in the processing pipeline shown in Figure 2 on page 4).

The input of the classification phase is:

- at the very beginning of the pipeline, the input facets correspond to a set of N operands $O_1, O_2, \dots O_n$. Each operand is represented by its (closed) boundary. The information of which facet comes from which operand is represented by sets $B(t)$ associated to each input triangular facet t :

$$B(t) = \{O_i | t \subset \partial O_i\}.$$

In practice, $B(t)$ can be represented by a bitvector associated with t , and the i -th bit indicates whether t belongs to ∂O_i . Note that the same input triangle may belong to the boundaries of several operands, for instance whenever two operands touch along a common surface. During the co-refinement phase, whenever two identical triangles t_1 and t_2 are merged into a single output triangle t , the associated sets are also merged: $B(t) = B(t_1) \cup B(t_2)$ (at the implementation level, in terms of bitvectors, they are ORed);

- a boolean expression $E(b_1, b_2, \dots b_N)$ that takes as an argument a vector of N booleans and that returns a boolean. For instance, for the union of two operands, this expression corresponds to $(b_1 \text{ or } b_2)$. For the intersection, it corresponds to $(b_1 \text{ and } b_2)$. For the difference, it corresponds to $(b_1 \text{ and not } b_2)$. It can have an arbitrary number of operands. For instance, in the example shown in Figure 2 P. 4, the expression is $E(b_1, b_2, b_3, b_4) = ((b_1 \text{ or } b_2 \text{ or } b_3) \text{ and not } b_4)$.

The classification phase aims at finding all the darts that are on the boundary of the object O_E defined by the boolean expression E . It is done in two phases:

- For each dart d , determine the set of objects $I(d) = \{O_i | d \in O_i\}$. The algorithm to compute the $I(d)$'s will be explained later. We consider that a dart d belongs to an object O_i if the triangle $t(d)$ it is incident to is included in O_i or if $t(d)$ is included in the boundary ∂O_i and has a normal vector that points inwards O_i . In other words, considering the two charts that cover the boundary of O_i (connected with α_3 links, see Figure 9-left), one of them is considered to be outside O_i and the other one inside O_i . Put differently, whenever one crosses an α_3 link from one of these darts, one moves from inside to outside or from outside to inside;

- once the $I(d)$'s are computed, one can characterize the darts on ∂O_E as follows:

$$d \in \partial O_E \Leftrightarrow \text{not } E(I(d)) \text{ and } E(I(\alpha_3(d))),$$

in other words, d is on the (external) boundary of O_E if d is outside O_E and if one gets inside O_E by traversing the α_3 link from d .

Let us see now how to compute the sets $I(d)$. We first consider how to classify all the darts in a single connected component, starting from a dart d , and knowing the set of objects $I(d)$ that contain d . Consider for now that d is on the external boundary of the connected component, hence $I(d) = \emptyset$.

classify_component(d,B)

input: a dart d and the set $I(d) = \{O_i | d \in O_i\}$

output: the sets $I(d')$ for $d' \in \langle \sigma_0, \alpha_2, \alpha_3 \rangle (d)$

-
- (1) push(S, d); mark(d)
 - (2) **while** S is not empty
 - (3) $d_1 \leftarrow \text{pop}(S)$
 - (4) **for** $d_2 \in \{\sigma_1(d_1), \alpha_2(d_1)\}$
 - (5) **if** d_2 is not marked **then**
 - (6) $I(d_2) \leftarrow I(d_1)$; push(S, d_2) ; mark(d_2)
 - (7) **end**
 - (8) **end**
 - (9) $d_3 \leftarrow \alpha_3(d_1)$; $t \leftarrow t(d_1)$
 - (10) **if** d_3 is not marked **then**
 - (11) $I(d_3) \leftarrow (I(d_1) \cap C_{B(t)}) \cup (C_{I(d_1)} \cap B(t))$
 - (12) push(S, d_3) ; mark(d_3)
 - (13) **end**
 - (14) **end**

The algorithm greedily traverses all the σ_1, α_2 and α_3 links from d . In steps (4-8), σ_1 and α_2 links are traversed, one stays within the same shell, hence $I(d)$ is propagated. In step (11), an α_3 link is traversed. In other words, one traverses a boundary, which means flipping the inside/outside status of the concerned operators $B(t)$. C_X denotes the complement of a set X . In terms of bit manipulation, it simply means XORing the bitvectors $I(d_1)$ and $B(t)$.

If the map is composed of several connected components, then one needs to do two different things for each connected component:

- *Find a dart d on the external boundary of the connected component.* To do so, among all the shells $\langle \sigma_1, \alpha_2 \rangle$ in the connected component, we select the one that encloses the largest volume. It is found in linear time;
- *compute $I(d)$.* The connected component may be an internal boundary (for instance if you compute the difference between two concentric balls). It could be also included inside another object. It is not possible to deduce $I(d)$ from the sole combinatorial information, it requires some geometric tests: first, $I(d)$ is initialized to \emptyset . Then, a ray is launched from a point in $t(d)$, and the inside/outside status of the operators $B(t)$ are flipped for each intersected triangle t (again, in terms of bit manipulation, this simply means XOR-ing $I(d)$ with $B(t)$).

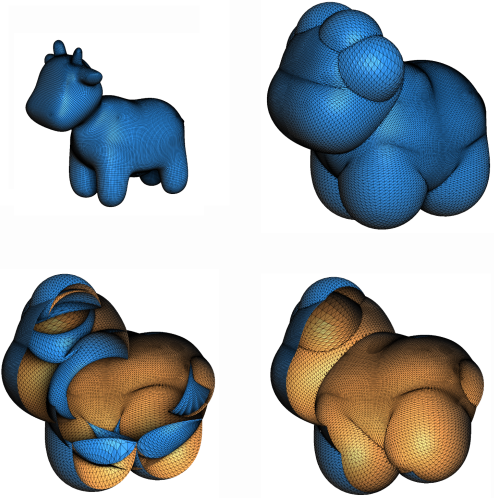


Figure 10: Using the Weiler model to remove the internal garbage after a (naive) offsetting operation.

To summarize, using the Weiler model, classification is mostly a combinatorial operation. Geometric computation is needed only in two places:

- radial-sorting one bundle per radial polyline;
- tracing one ray per connected component

Other mesh repair operation: remove internal “garbage”.

Besides providing an efficient combinatorial data structure for implementing arbitrary boolean operations, the Weiler model can also be used to implement other mesh repair operations. For instance, in 3D mesh generation, one often wants to extract the “outer skin” from a (possibly self-intersecting) polygon soup. As shown in Figure 10, one may also need to remove the internal “garbage” after performing a naive offsetting operation (here all vertices were simply moved a certain distance along their normal vectors). To do so, one possibility is to compute the union of everything, however, if the input is a polygon soup, it will not be easy to tag each individual primitives. Another possibility is to extract the outer shell of all connected component and keeping the ones that are not included in other components. This operation is trivial to implement from the two algorithms of the previous paragraph (the one that determines the outer shell and the one that traces a ray).

2.2.4 Simplifying. The last step of our pipeline is the simplification of co-planar facets, (step 5 in Figure 2 P. 4), recalled in Figure 11-A: the border of the volume defined by the boolean expression may present the “scars” of intersection that were computed during the co-refinement phase, that are not necessarily needed in the final mesh. One possibility to remove these scars would be to keep in each triangle of the co-refinement a reference to the input triangle, so that triangles coming from the same initial triangle could be merged in a post-processing phase. However, the input data may also contain poorly triangulated planar areas, worth remeshing, such as the example shown in Figure 11-B). The regions composed of co-planar facets are detected by greedily traversing them, using

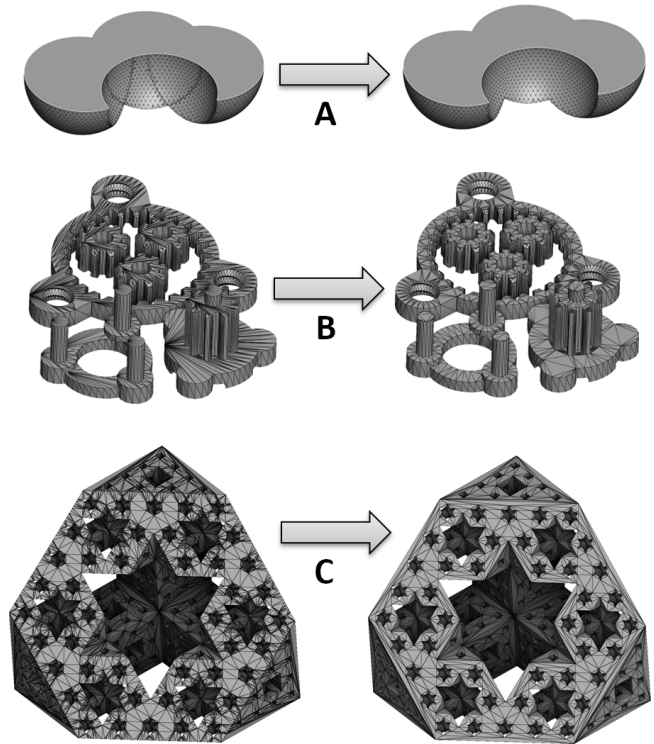


Figure 11: Simplification of the coplanar facets

an exact predicate that tests the co-linearity between the normal vectors of two adjacent facets. Then, the borders of these regions are extracted. Finally, the edges of the borders are inserted in a constrained Delaunay triangulation, using the same algorithm (and the same code) as in the co-refinement phase. Finally, the triangles in the external zone and in the (potential) internal pocket are discarded thanks to a greedy traversal.

In addition, before inserting the border edges into the constrained Delaunay triangulation, the borders can be simplified: one can discard a vertex of the border provided that it is aligned with its predecessor and successor along the border and provided that it does not appear somewhere else in the mesh. The effect of this simplification is shown in Figure 11-C.

2.3 Summary of the algorithmic pipeline architecture

Before diving into the details of the arithmetic kernels, let us take a step backwards and see how the different components mesh together. As mentioned in the introduction, there are many possible choices for the data structure that store and share combinatorial information between the stages of the pipeline, and one needs to find the right balance: on the one hand, storing more combinatorial information may improve performance. On the other hand, introducing more data structure makes the system more complicated, and more difficult to maintain. The choices that I made are summarized in Figure 12. The data shared by all stages of the pipeline is simply an indexed triangulated mesh. In addition, some stages share

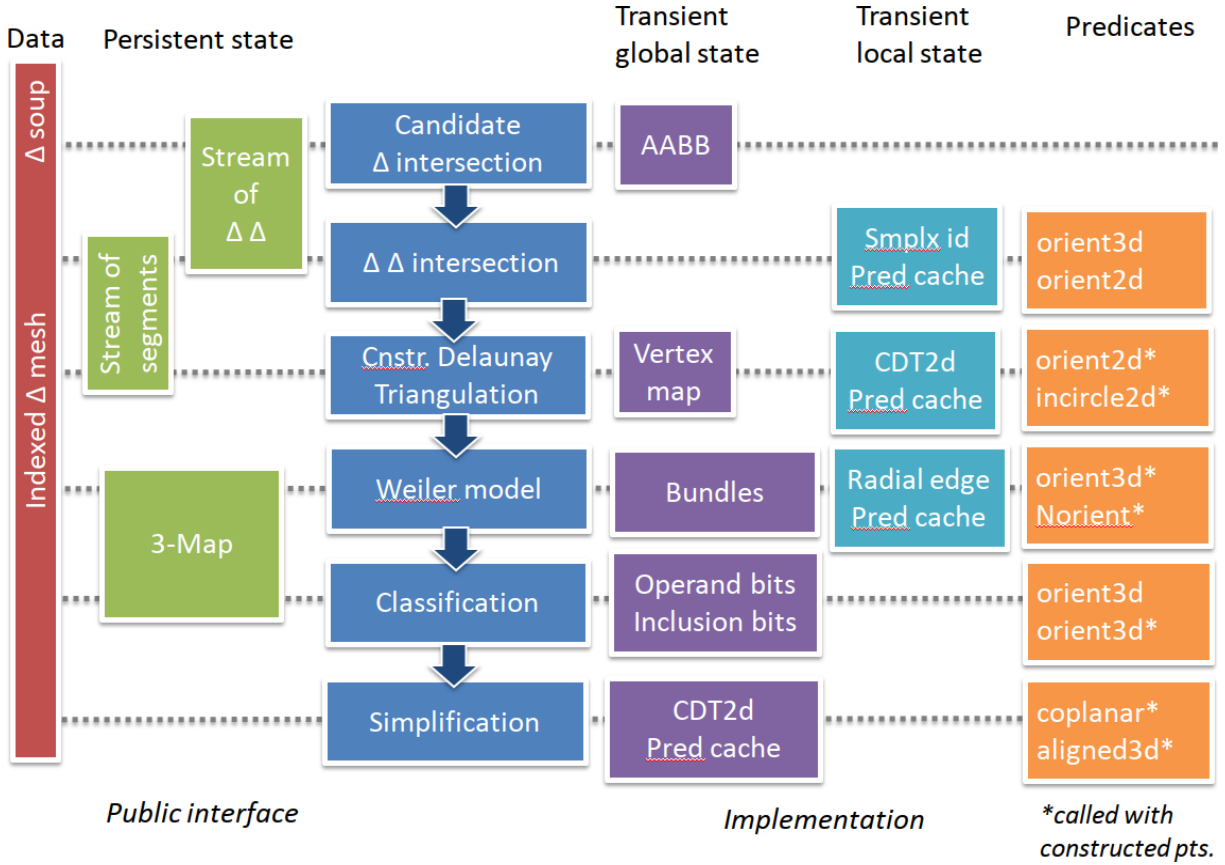


Figure 12: Global architecture of the algorithm

a *persistent stage*. For instance, the AABB sends a stream of candidate triangle intersection pairs to the triangle-triangle intersection, that in turn sends a stream of segments to the constrained Delaunay triangulation. The Weiler model and the classification phase share a 3-map. This defines the public interface of the pipeline stages (left part of the figure). Each stage has an internal state (right part of the figure), that disappears at the end of the stage (transient). A part of it is global in the mesh, and a part of it is more local, attached to individual elements (or small group of elements) of the mesh. Finally, each stage uses some predicates, some of them applied to the original vertices, and some of them to the computed intersections. In this architecture, the combinatorial information communicated between the stages is very reduced, which makes it easier to develop, unit-test and maintain each individual stage. It is made possible by pushing a significant part of the complexity towards the exact representation of the points and the predicates, detailed in the next section.

2.4 Nuts and bolts: two arithmetic kernels

I shall now give more details about the arithmetic kernels. The reader may skip this section in a first read. This section contains details that I considered worth sharing, about how to implement arbitrary precision numbers and about how to derive the formulas for the predicates acting on them, together with non-trivial

details that have important consequence on performance. I tested two different version, one based on arithmetic expansions, and the other one based on multiprecision floating point arithmetics. Each kernel provides an `exact_nt` number type, that supports addition, subtraction and product, 2d and 3d vectors with cartesian and homogeneous coordinates represented by `exact_nt`, as well as the standard predicates `orient_2d`, `orient_3d`, and symbolically perturbed `in_circle`. Each kernel also provides lexicographic points comparison, used to create the global vertex table (see Section 2.1.3) and used by the symbolic perturbations. For both kernel, I detail how numbers are represented, and how the different predicates are implemented.

2.4.1 The expansion-based arithmetic kernel.

Arithmetic expansions. With arithmetic expansions (explained in great detail in [37, 39] and mentioned in Section 1.3), each number is represented by an array of floating-point numbers called *components*. The represented number corresponds to the sum of the components. In addition, these components are sorted by decreasing exponents, and satisfy a special property: they are *non-overlapping*, that is, the exponents and the bits sets in the mantissa are such that the sign is determined by the first component. Arithmetic expansions are based on the *two-sum* algorithm [34], or its fast version [17], that computes the rounded sum x_1 of two numbers a and b ,

and the exact round-off error x_2 , as follows:

$$\begin{aligned} x_1 &\leftarrow a \oplus b \\ x_2 &\leftarrow b \ominus (x_1 \ominus a). \end{aligned}$$

where \oplus and \ominus denote the addition and subtraction of IEEE754 floating point numbers rounded to nearest.

By properly orchestrating these operations (as well as a more complicated *two-prod* operation that computes the same information for products), one can implement addition, subtraction and product for expansions of arbitrary lengths, and use them to implement exact geometric predicates, as explained by Shewchuk in [37, 39]. The *distillation* operation required to compute the product of expansions of arbitrary lengths, also evoked in the references above, is implemented in [23].

The idea here is to test whether arithmetic expansions can be used to implement *exact constructions*. In our case, these exact constructions are used to compute the new intersection points. Note also that some predicates take these constructed points as inputs, in the constrained Delaunay triangulations and in the radial sort. This means that the algebraic operations on the constructed point's coordinates are going to be chained. This chaining / nesting of expressions that is much deeper than with the classical usage of arithmetic expansions has two consequences:

- with arithmetic expansions, the representation of the same number is non-unique: in the extreme case, one could imagine using a single component for each non-zero bit in the number. If not enough care is taken, the length of the stored numbers grow larger and larger, as well as computation time;
- arithmetic expansions are not limited in length, but it is not sufficient to ensure that arbitrary numbers can be manipulated: exponents are stored with a limited number of bits (11 bits in double precision), and overflow and underflow may occur when multiplying very large or very small numbers. This limit is quickly reached, for instance, when using the `in_circle` predicate on points coming from the intersection of several triangles.

Both bottlenecks can be mitigated as follows:

Compression. Compression is an operation that takes an expansion and that returns a more compact expansion with the same value. It is described in Section 2.8 of [39], and can be summarized as in the algorithm below⁸.

compress(e)

input/output: e : an expansion (compressed in-place)

```

(0)   $m \leftarrow \text{length}(e)$ 
(1)   $Q \leftarrow e_m$ 
(2)   $bottom \leftarrow m$ 
(3)  for  $i = m - 1$  to 1
(4)     $(Q, q) \leftarrow \text{fast\_two\_sum}(Q, e_i)$ 
(5)    if  $q \neq 0$  then
(6)       $e_{bottom} \leftarrow Q$ 
(7)       $bottom \leftarrow bottom - 1$ 
(8)    end
(9)  end
(10)  $e_{bottom} \leftarrow Q$ 
(11)  $top \leftarrow 1$ 
(12) for  $i = bottom + 1$  to  $m$ 
(12)   $(Q, q) \leftarrow \text{fast\_two\_sum}(e_i, Q)$ 
(13)  if  $q \neq 0$  then
(14)     $e_{top} \leftarrow q$ 
(15)     $top \leftarrow top + 1$ 
(16)  end
(17) end
(18)  $e_{top} \leftarrow Q$ 
(19)  $\text{set\_length}(e, top)$ 

```

Compression proceeds by sweeping the expansion twice, in both directions, first from largest to smallest component, then from smallest to largest, “swallowing” a component each time the rounded sum of two successive components is exact (test $q \neq 0$ line 7 and 16). Since the speed of the arithmetic operations dramatically depend on the length of the involved expansions, this function is called before each complicated operation, such as computing a determinant, and before storing a constructed point. It is worth it, because expansion product costs a lot (in $O(m \times n)$, product of expansion lengths).

Orientation predicates. I shall now explain how to compute the different predicates that we need. The orientation predicates (`orient_2d` and `orient_3d`) are classical. The only subtlety is that the points are in homogeneous coordinates. Given three points $\mathbf{p}_0, \mathbf{p}_1, \mathbf{p}_2$ with homogeneous coordinates ($\mathbf{p}_i = [x_i \ y_i \ w_i]$), the predicate `orient_2d` writes:

$$\text{orient_2d}(\mathbf{p}_0, \mathbf{p}_1, \mathbf{p}_2) = \text{sign}(U_w) \text{sign}(V_w) \text{sign} \begin{vmatrix} U_x & U_y \\ V_x & V_y \end{vmatrix}.$$

where:

$$\begin{aligned} U &= [x_1 - x_0 \ y_1 - y_0 \ w_1] && \text{if } w_1 = w_0 \\ U &= [w_0x_1 - w_1x_0 \ w_0y_1 - w_1y_0 \ w_0w_1] && \text{otherwise} \\ V &= [x_2 - x_0 \ y_2 - y_0 \ w_2] && \text{if } w_2 = w_0 \\ V &= [w_0x_2 - w_2x_0 \ w_0y_2 - w_2y_0 \ w_0w_1] && \text{otherwise} \end{aligned}$$

and `orient_3d` is written similarly.

Note: one could have used instead the alternative expression:

$$\text{orient_2d}(\mathbf{p}_0, \mathbf{p}_1, \mathbf{p}_2) = \begin{vmatrix} x_0 & y_0 & w_0 \\ x_1 & y_1 & w_1 \\ x_2 & y_2 & w_2 \end{vmatrix}$$

⁸I think there is a typo in the original article, line 14 should read $h_{top} \leftarrow q$ (small q and not capital Q). I think that this error was overlooked before because compression is mostly needed when cascading operations, as done here since expansions are used in exact constructions, and it was probably not done before.

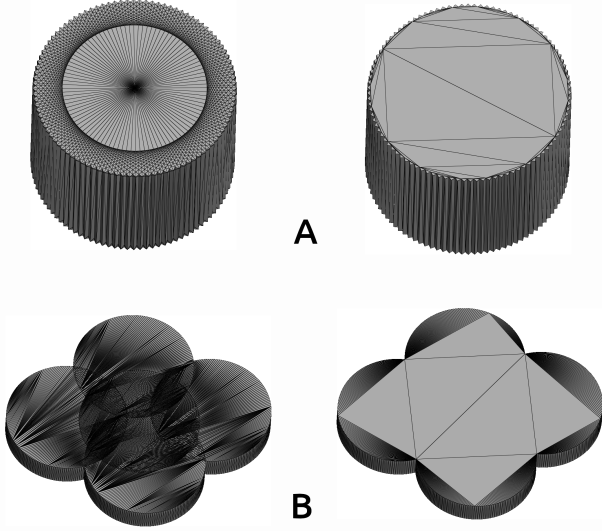


Figure 13: Examples of mesh unions computed with arithmetic expansions. A: union of 50 rotated cubes. B: union of four cylinders, with many coplanar facets. Both examples are computed without (left) and with (right) simplification of coplanar facets.

but it is in general preferable to use expressions with coordinate differences, leading to much smaller expansions (see [37, 39]). The effect is even more dramatic in our case, where input points come from exact constructions.

All computations are done using arithmetic expansions. To speed-up computation in the easy cases, a filter based on interval arithmetics is used. To convert an expansion e into an interval, that is, finding the tightest interval that contains the exact number represented by e , I add all components of e to the interval in decreasing magnitude order, stop as soon as next component is smaller than ulp, then expand interval by 1 ulp.

The in-circle predicate and its symbolic perturbation. The in-circle predicate is more subtle, because it has higher degree. Clearly one could directly implement the classical formula (written here with cartesian coordinates):

$$\text{in_circle}(\mathbf{p}_0, \mathbf{p}_1, \mathbf{p}_2, \mathbf{p}_3) = \text{sign} \begin{vmatrix} x_0 & y_0 & x_0^2 + y_0^2 & 1 \\ x_1 & y_1 & x_1^2 + y_1^2 & 1 \\ x_2 & y_2 & x_2^2 + y_2^2 & 1 \\ x_3 & y_3 & x_3^2 + y_3^2 & 1 \end{vmatrix}.$$

However, we remind that the higher degree in this expression can be a problem in our case, because our input points come from constructions, and nesting too many operations with arithmetic expansions can lead to overflow or underflow due to the limited number of bits to represent an exponent. The multi-precision kernel presented in the next section does not have this limitation, but let us see whether this issue can be mitigated with arithmetic expansions. There exists a more general version of the `in_circle` predicate,

used to construct power diagrams (also called Laguerre diagrams) and their duals (called regular triangulations). This predicate takes additional weights $\psi_0, \psi_1, \psi_2, \psi_3$ as arguments and writes:

$$\text{in_circle_weighted}(\mathbf{p}_0, \mathbf{p}_1, \mathbf{p}_2, \mathbf{p}_3, \psi_0, \psi_1, \psi_2, \psi_3) = \text{sign} \begin{vmatrix} x_0 & y_0 & x_0^2 + y_0^2 - \psi_0 & 1 \\ x_1 & y_1 & x_1^2 + y_1^2 - \psi_1 & 1 \\ x_2 & y_2 & x_2^2 + y_2^2 - \psi_2 & 1 \\ x_3 & y_3 & x_3^2 + y_3^2 - \psi_3 & 1 \end{vmatrix}.$$

So imagine now that you rewrite the `in_circle` predicate and pass to it additional arguments l_i as follows:

$$\text{in_circle_l}(\mathbf{p}_0, \mathbf{p}_1, \mathbf{p}_2, \mathbf{p}_3, l_0, l_1, l_2, l_3) = \text{sign} \begin{vmatrix} x_0 & y_0 & l_0 & 1 \\ x_1 & y_1 & l_1 & 1 \\ x_2 & y_2 & l_2 & 1 \\ x_3 & y_3 & l_3 & 1 \end{vmatrix}.$$

If you use $l_i = x_i^2 + y_i^2$, you obtain exactly the same result as `in_circle`. Now, if you use instead $l_i = \text{round_to_nearest}(x_i^2 + y_i^2)$, then what you obtain is the same result as `in_circle_weighted`, with $\psi_i = \text{round_to_nearest}(x_i^2 + y_i^2) - (x_i^2 + y_i^2)$. While it is not exactly the same result as `in_circle`, what you obtain in the end is still a well-defined object, a Regular Triangulation (dual of power diagram), very similar to the Delaunay triangulation, except for a few flipped edges, and more importantly, provided that always the same l is used for the same point, and with adapted symbolic perturbation, the triangulation remains uniquely defined. There is however an important difference: if `in_circle_l`($\mathbf{p}_1, \mathbf{p}_2, \mathbf{p}_3, \mathbf{p}_4, l_1, l_2, l_3, l_4$) is negative, it does not necessarily imply that $(\mathbf{p}_1, \mathbf{p}_2, \mathbf{p}_3, \mathbf{p}_4)$ forms a convex quadrilateral. In the constrained Delaunay triangulation, this condition needs to be explicitly tested before flipping an edge.

We shall now see how to write the predicate for points with homogeneous coordinates and the associated symbolic perturbation.

Take the determinant in `in_circle_l` above, subtract the last row from the first three rows then develop w.r.t. the fourth row:

$$\text{in_circle_l} = \text{sign} \begin{vmatrix} x_0 - x_3 & y_0 - y_3 & l_0 - l_3 \\ x_1 - x_3 & y_1 - y_3 & l_1 - l_3 \\ x_2 - x_3 & y_2 - y_3 & l_2 - l_3 \\ x_3 & y_3 & l_3 \end{vmatrix}.$$

We now need to take into account that the points are represented with homogeneous coordinates, and we need to find an expression without any division.

$$\text{using : } \begin{cases} (X_{i+1}, Y_{i+1}, W_{i+1}) & = \mathbf{p}_i - \mathbf{p}_3 & \text{in homo. coords.} \\ L_{i+1} & = l_i - l_3 \end{cases}$$

$$\text{one gets: } \text{in_circle_l} = \text{sign} \begin{vmatrix} X_1/W_1 & Y_1/W_1 & L_1 \\ X_2/W_2 & Y_2/W_2 & L_2 \\ X_3/W_3 & Y_3/W_3 & L_3 \end{vmatrix}.$$

Developping along the last column, factoring the W_i 's out, and multiplying everything by $W_1 W_2 W_3$, one finally obtains:

$$\text{in_circle_l} = \text{sign}(W_1) \times \text{sign}(W_2) \times \text{sign}(W_3) \times$$

$$\text{sign} \left(L_1 W_1 \begin{vmatrix} X_2 Y_2 \\ X_3 Y_3 \end{vmatrix} - L_2 W_2 \begin{vmatrix} X_1 Y_1 \\ X_3 Y_3 \end{vmatrix} + L_3 W_3 \begin{vmatrix} X_1 Y_1 \\ X_2 Y_2 \end{vmatrix} \right).$$

I am using Simulation of Simplicity [10] to consistently take a decision when the quantity above is zero. I consider that the points $\mathbf{p}_0, \mathbf{p}_1, \mathbf{p}_2, \mathbf{p}_3$ are geometrically sorted, which defines local indices i_0, i_1, i_2, i_3 (a permutation of $\{0, 1, 2, 3\}$). I am using for that the lexicographic order on the point's cartesian coordinates $x_i/w_i, y_i/w_i$ (more on this in the next paragraph). Now I consider that the lengths parameters l_0, l_1, l_2, l_3 are replaced with $l_0 + \epsilon^{i_0}, l_1 + \epsilon^{i_1}, l_2 + \epsilon^{i_2}, l_3 + \epsilon^{i_3}$ for a small ϵ . The perturbed predicate is then defined by the sign of the first non-zero coefficient of ϵ^{ik} . They are easy to find, using the following expression of `in_circle_1` and developing it with respect to the third row and keeping only the coefficients in ϵ^{ik} :

$$\begin{aligned} \text{in_circle_1} &= \begin{vmatrix} x_0 & y_0 & l_0 + \epsilon^{i_0} & 1 \\ x_1 & y_1 & l_1 + \epsilon^{i_1} & 1 \\ x_2 & y_2 & l_2 + \epsilon^{i_2} & 1 \\ x_3 & y_3 & l_3 + \epsilon^{i_3} & 1 \end{vmatrix} \\ &= \dots + \epsilon^{i_0} \begin{vmatrix} x_1 & y_1 & 1 \\ x_2 & y_2 & 1 \\ x_3 & y_3 & 1 \end{vmatrix} - \epsilon^{i_1} \begin{vmatrix} x_0 & y_0 & 1 \\ x_2 & y_2 & 1 \\ x_3 & y_3 & 1 \end{vmatrix} + \\ &\quad \epsilon^{i_2} \begin{vmatrix} x_0 & y_0 & 1 \\ x_1 & y_1 & 1 \\ x_3 & y_3 & 1 \end{vmatrix} - \epsilon^{i_3} \begin{vmatrix} x_0 & y_0 & 1 \\ x_1 & y_1 & 1 \\ x_2 & y_2 & 1 \end{vmatrix} \end{aligned}$$

In homogeneous coordinates, the signs of the coefficients of ϵ^{ik} can be computed as follows:

$$\begin{aligned} \text{sign} \begin{vmatrix} x_1/w_1 & y_1/w_1 & 1 \\ x_2/w_2 & y_2/w_2 & 1 \\ x_3/w_3 & y_3/w_3 & 1 \end{vmatrix} &= \\ \text{sign} \left(w_1 \begin{vmatrix} x_2 & y_2 \\ x_3 & y_3 \end{vmatrix} - w_2 \begin{vmatrix} x_1 & y_1 \\ x_3 & y_3 \end{vmatrix} + w_3 \begin{vmatrix} x_1 & y_1 \\ x_2 & y_2 \end{vmatrix} \right) &\times \\ \text{sign}(w_1) \times \text{sign}(w_2) \times \text{sign}(w_3) & \end{aligned}$$

Geometric sorting and geometric indexing. The global vertex table (see Section 2.1.3) and the symbolic perturbation introduced above need a total order on the points. I am simply using the lexicographic order, based on a function that compares the cartesian coordinates of two points. Since our points are stored with homogeneous coordinates, it means comparing rationals. What we need is a new predicate:

$$\begin{aligned} \text{ratio_compare}(x_1, w_1, x_2, w_2) &= \text{sign} \left(\frac{x_1}{w_1} - \frac{x_2}{w_2} \right) \\ &= \text{sign}(w_1) \times \text{sign}(w_2) \times \text{sign}(w_2x_1 - w_1x_2). \end{aligned}$$

Since computing $w_2x_1 - w_1x_2$ takes significant time with long expansions, the predicate is optimized in three particular cases where the result is trivial and where this computation can be avoided:

- if x_1 and x_2 are both zero;
- if the signs of x_1/w_1 and x_2/w_2 differ;
- if $w_1 = w_2$.

The expansion-based arithmetic kernel works reasonably well in practice, and can be used for co-refinement operations. The example shown in Figure 13 with many coplanar surfaces demonstrates how it successfully generates a unique triangulation in them. For both example, the Euler-Poincaré characteristic is 2, as expected. Hence, the `in_circle_1` predicate makes it possible to push the limits of

what can be computed with arithmetic expansions. Co-refinements can be computed nearly with all models of the Thingi10K database.

However, one still reaches the limit when attempting to create the Weiler model: the involved predicates compute cross-products between vectors joining constructed points, and then dot product between those. Remember that the points are themselves the result of intersections. I instrumented the code to output an histogram of the lengths of the expansions, and they can be as long as 65000. This is not that surprising, knowing that each operation can potentially double the length of the expansions, this corresponds to 16 nested levels. Thanks to compression, this seldom occurs (no more than a few times in multi-million element meshes). Besides the time and space requirement for these very long expansions, a more important problem is that they can yield overflows and underflows when computing products with them. For instance, using the expansion-based kernel, it can successfully evaluate the CSG trees in `example0001.csg` to `example0020.csg` in the OpenSCAD category of the ThingiCSG testsuite (see 3.2 below), but it fails with all CSG trees between `example0021.csg` to `example0024.csg`.

2.4.2 The multiprecision floating-point arithmetic kernel. For this reason, and because the algorithm is used in production by the Tessel company, I implemented and tested an alternative kernel, that does not have the limitations of the expansion-based kernel mentioned above.

Multiprecision floating-point arithmetics. The kernel is based on multi-precision integers, implemented in the GNU Multiple Precision library (GMP), similarly to what is done in CGAL [46]. As in CGAL, I represent a floating point number with a mantissa m stored as a multi-precision signed integer from GMP (`mpz_t`) and a 32 bits exponent e . The represented number is $m \times 2^e$. To ensure the uniqueness of the representation, m is constrained to have no trailing zero (its least significant bit is always 1), with the exception of 0, always represented as 0^0 . GMP provides all the necessary functions (initialization from integer, adding, subtracting, product, left and right shift, comparisons). As compared to CGAL, I optimized some operations, such as equality (compare sign, then exponent, then mantissa only if they were the same), comparisons (easy answer if signs differ), and comparison with special values such as 0 and 1. It has a non-negligible impact in our context, where many operations are nested.

To convert a multiprecision floating-point number into an interval, one first initializes both bounds of the interval to the approximation of the number as a standard floating-point number. If it did not fit in the floating-point number, then the interval is enlarged by 1 ulp towards $-\infty$ or $+\infty$ depending on the sign of the number.

The predicates. The orientation predicates use the same formulas as in the expansion-based kernel. For the `in_circle` predicate, one could reuse the formulas of the expansion-based kernel, and inject the exact computation of $l_i = x_i^2 + y_i^2$ into them, however, it is better to make *difference of coordinates* appear in the computed determinants, since it reduces cancellation errors in general, and improves the performance of the arithmetic filter based on intervals. Let's start from the original expression of the predicate, recalled here:

$$\text{in_circle} = \text{sign} \begin{vmatrix} x_0 & y_0 & x_0^2 + y_0^2 & 1 \\ x_1 & y_1 & x_1^2 + y_1^2 & 1 \\ x_2 & y_2 & x_2^2 + y_2^2 & 1 \\ x_3 & y_3 & x_3^2 + y_3^2 & 1 \end{vmatrix}.$$

Then, you translate \mathbf{p}_3 to the origin and develop with respect to the last row:

$$\text{in_circle} = \text{sign} \begin{vmatrix} x_0 - x_3 & y_0 - y_3 & (x_0 - x_3)^2 + (y_0 - y_3)^2 \\ x_1 - x_3 & y_1 - y_3 & (x_1 - x_3)^2 + (y_1 - y_3)^2 \\ x_2 - x_3 & y_2 - y_3 & (x_2 - x_3)^2 + (y_2 - y_3)^2 \\ 1 & 1 & 1 \end{vmatrix}.$$

This determinant is very similar to the one obtained in the previous subsection, with the difference that the coefficients in the third column are $(x_i - x_3)^2 + (y_i - y_3)^2$ instead of $(x_i^2 + y_i^2) - (x_3^2 + y_3^2)$. It may be surprising that both expressions are equivalent, but remember that the first one was obtained by row manipulations, and the second one by geometric reasoning, both types of transform leaving the determinant invariant.

Rewriting the determinant in terms of the homogeneous coordinates (X_i, Y_i, W_i) of $\mathbf{p}_i - \mathbf{p}_3$ and $L_i = X_i^2 + Y_i^2$, one gets:

$$\text{in_circle} = \text{sign} \left(\frac{1}{W_0^2 W_1^2 W_2^2} \begin{vmatrix} W_0 X_0 & W_0 Y_0 & L_0 \\ W_1 X_1 & W_1 Y_1 & L_1 \\ W_2 X_2 & W_2 Y_2 & L_2 \end{vmatrix} \right).$$

The positive factor can be dropped (we are only interested in the sign). Developing w.r.t. the last column, one finally gets:

$$\text{in_circle} = \text{sign} \left(L_0 W_1 W_2 \begin{vmatrix} X_1 & Y_1 \\ X_2 & Y_2 \end{vmatrix} - L_1 W_0 W_2 \begin{vmatrix} X_0 & Y_0 \\ X_2 & Y_2 \end{vmatrix} + L_2 W_0 W_1 \begin{vmatrix} X_0 & Y_0 \\ X_1 & Y_1 \end{vmatrix} \right)$$

Geometric sorting and geometric indexing. As with the expansion-based kernel, we need a total order on the points. Clearly we could use exactly the same formula as what we did for expansions, but we can exploit the uniqueness of the representation (that we did not have with expansions). The representation of 3D points stored with homogeneous coordinates (x, y, z, w) is normalized as follows:

- x, y, z, w are divided by their mutual gcd;
- w is positive;
- the exponent of w is zero.

With this convention, the representation of a point is unique, and one can simply use the lexicographic order on x, y, z, w , forgetting their geometric nature. Clearly, it will give a different order as compared to the lexicographic order on $x/w, y/w, z/w$ used before, but it is not a problem since the only thing we need to have for the symbolic perturbation and for the global vertex table to work is a total order. We also noticed that we are not obliged to pre-shift the numbers so that w 's exponent is zero, instead of that we pass the shifts to the comparison function, and shift by their difference only. It makes both the spatial indexing and predicates significantly more efficient (else they keep shifting the same numbers left and right).

ID	Cherchi	Ours	Ours	Ours
	et.al.	expansions Delaunay	multi prec. Delaunay	multi prec. no Del.
252784	104	580	89	78
1016333	868	X	115	112
55928	87	298	46	37
12368052	120	541	152	114
498461	19	123	21	16
338910	8	103	13	10
252785	24	106	16	13
498460	12	92	12	11
242236	50	18	24	20
242237	49	11	22	21

Table 1: Timings (in seconds) for the 10 models from Thingi10K with the largest number of intersections

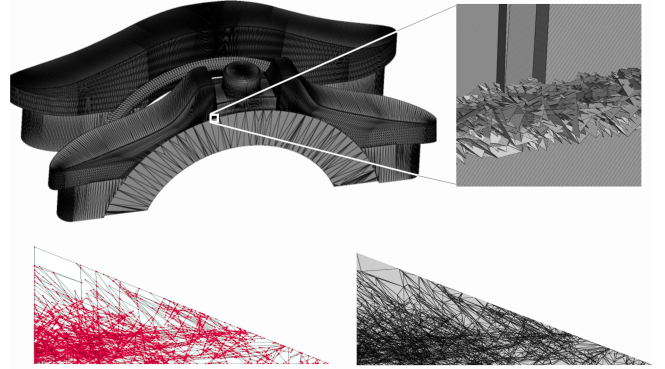


Figure 14: One of Thingi10k's monsters, thing 996816. This mesh has a huge number of intersections, most of them located in the highlighted zone. It has up to several thousand intersections in the same triangle.

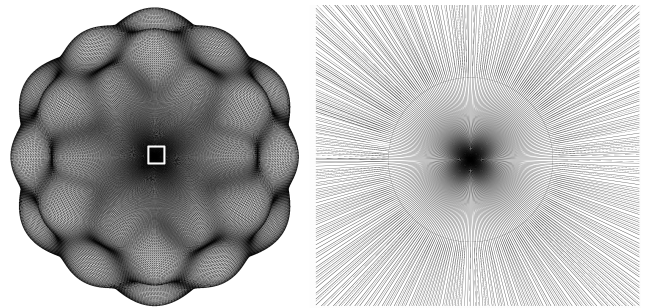


Figure 15: Another monster from Thingi10k, thing 101633. This mesh stresses the arithmetic kernel a lot, with a large number of intersections located near a pole.

3 TESTS

3.1 Thingi10K

I shall now report some timings and statistics, first with Thingi10K [52], a database with 10000 meshes. In the database, 4523 of them

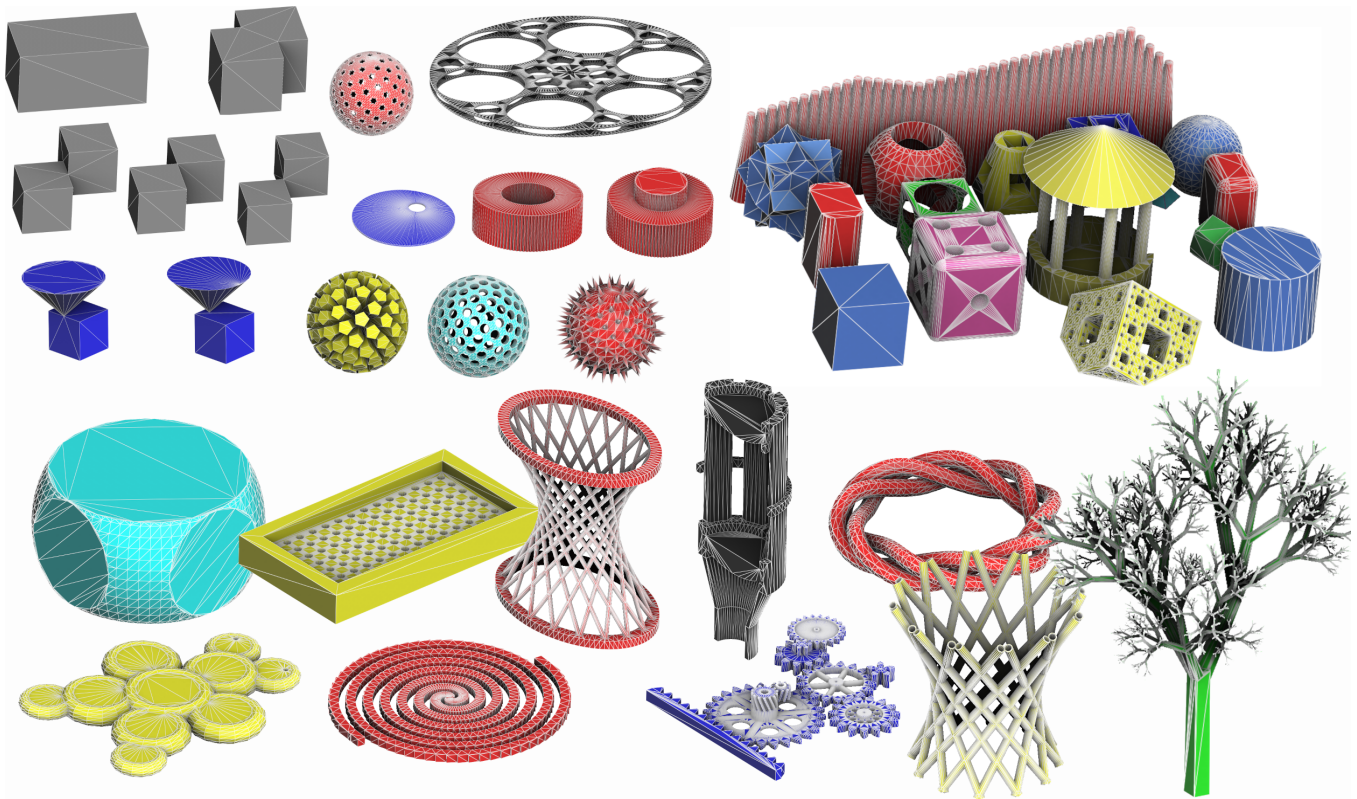


Figure 16: ThingiCSG: a collection of openSCAD files from different sources

have intersections. The complete subset of models with intersections is processed in 1h 45min. One of them (996816, shown in Figure 14) is particular and takes 1271s (20 min) to be processed. It has up to several thousands intersections in the same triangle. This is because it has in a tiny zone a “3D grid of triangles”, that is, exactly the best method to create $O(N^3)$ intersections with N triangles. It is a good crash test for all the components of a mesh intersection algorithm, in particular the constrained Delaunay triangulation. Timings for the next 10 meshes with the largest number of intersections are reported in Table 1. The first column gives the timings for the state of the art [4]. The second column corresponds to the kernel based on arithmetic expansions. For one of the models (101633, displayed in Figure 15), this kernel could not compute a correct result, because underflows were encountered. It is explained by the shape of the triangles that have intersections, that are very skinny and intersecting near the pole. They generate arithmetic operations that combine very large and very small numbers. This also explains the long timing obtains with previous work on this model. The third column reports the timings obtained with the multi-precision floating point kernel. As can be seen, for the largest models, timings are faster than with [4], and for some of them they are slower. Faster timings are explained by our exact constructions: in a certain sense, indirect predicates need to redo the same computations several times, whereas exact constructions act as a “cache”. Slower timings are explained by the constrained *Delaunay* triangulations that I compute, that involve the rather costly `in_circle`

predicate. As far as 101633 is concerned, carefully designing the arithmetic kernel and the associated predicates as done in Section 2.4.2 has a significant impact on the performance. The fourth column reports the timings obtained with the multi-precision floating point kernel and constrained triangulations (not Delaunay). It lets us see much it costs to ensure the Delaunay property. With this kernel, timings are almost always faster as compared to previous work. Note that we loose the uniqueness of the triangulation, and therefore one would need a pocket identification algorithm as in [4] to make a fair comparison.

3.2 ThingiCSG

To test the Weiler model and classification algorithm, I collected 83 files in the OpenSCAD format from different locations (some of them are displayed in Figure 16):

- the OpenSCAD examples and test suite [51], with examples of increasing complexity;
- an OpenSCAD tutorial [13], with more complicated examples;
- the files from my non-regression test suite, with small but challenging examples, with degeneracies, as well as larger ones, such has the “Finobunny sphere” on the first page.

OpenSCAD has two different file formats: the `.scad` format, that corresponds to a complete programming language, and the `.csg`

ID	ours	CGAL NEF	CGAL coref.	manifold
00_WarmUpExercise	<1	1	1	<1
01_Newbie2Guru15min	2	15	1	1
03_TeachingScript...	15	108	29	2
13_hyperboloid	3	25	8	1
14_LightSaber	1	10	3	<1
15_FamilyTreePendant	1	8	1	<1
16_Ring5	1	25	7	<1
17_Tree	131	1721	11	2
19_LEDlamp	6	151	96	1
20_ElectricCircuit...	2	35	20	1
21_BasWheel	6	21	6	<1

Table 2: Timings (in seconds) for the Presentation collection of ThingiCSG.

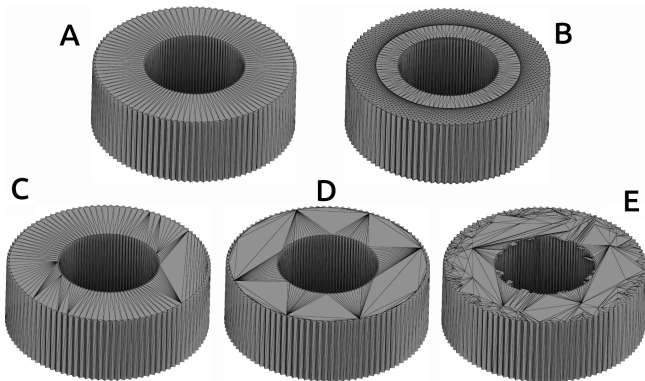


Figure 17: ThingiCSG’s nasty_gears_1 model, composed of the difference between two sets of 50 rotated cubes. This creates many co-planar facets. A: our result; B: our result without simplification of co-planar facets; C: CGAL NEF result; D: CGAL corefinement result; E: “manifold” kernel result.

format, limited to a subset of the OpenSCAD language, corresponding to “flat CSG trees”, with only primitive and CSG operations. I implemented a parser for the .csg format, that makes it easier to test CSG operations (an alternative would have been to implement a backend for OpenSCAD). One can use OpenSCAD to convert from the .scad to the .csg file format.

Both OpenSCAD files and the .csg parser will be made available in a new thinggiCSG repository, to make it easy to test and benchmark new research projects on mesh CSG.

I shall now give some statistics and comparisons, using:

- the algorithm presented in this article.
- the default OpenSCAD backend, based on CGAL NEF polyhedra [12],
- the OpenSCAD backend, based on CGAL co-refinement [16],
- the “manifold” OpenSCAD backend [19], based on [41]

On the OpenSCAD examples collection (Figure 16 top right), that has 29 files, the four kernels take 1s and less on each file, except the NEF kernel, that takes 28s on example006.scad and

ID	ours	CGAL NEF	CGAL coref.	manifold
christmas_ball	6	71	4	1
cube_cone_1..2	<1	<1	<1	<1
demo_reel	8	29	121	1
demo_reel_u..	5	18	117	<1
demo_reel_u..n..	2	8	2	<1
fibonacci_cylinders	<1	4	<1	<1
fishy_sphere	45	513	17	1
golf	5	176	3	1
hollow_ball_bunny	8	171	6	1
hollow_ball	3	50	3	1
multi_rot_cube	43	15	13	<1
nasty_gear_0	2	9	2	<1
nasty_gear_1	4	11	2	<1
nasty_gear_2	5	9	2	<1
nasty_gear_3	4	9	3	<1
nasty_gear_4	4	10	2	<1
seven_sins_2	2	9	24	<1
seven_sins_3	3	19	235	<1
seven_sins_4	3	20	244	<1
seven_sins	2	6	1	<1
spiky	<1	14	<1	<1
three_cubes	<1	<1	<1	<1
two_cubes_1..5	<1	<1	<1	<1
two_cylinders_1	4	2	29	<1
two_cylinders_2	1	1	1	<1

Table 3: Timings (in seconds) for the Basic collection of ThingiCSG.

ID	ours	CGAL coref.	manifold
fibonacci_bunny_union	749	1482	380
fibonacci_bunny_diff.	985	1450	311
fibonacci_sphere_20	3	5	1
fibonacci_sphere_100	44	69	18
fibonacci_sphere_200	200	292	72
fibonacci_sphere_500	2225	X	385

Table 4: Timings (in seconds) for the Large collection of ThingiCSG.

example024.scad, and that takes a few seconds on example010.scad, example018.scad and above.

The statistics for the four kernel on the Presentation collection (Figure 16 bottom) are reported in Table 2, and the statistics for the Basic collection, with custom small-but-challenging models that I created, are shown in Table 3. As can be seen, the “manifold” kernel is always the fastest. Our method is often faster than the co-refinement kernel, except in a small number of cases. A visual comparison on one of the examples (nasty_gears_1) is shown in Figure 17. This example is challenging, because it is made of the difference between two sets of 50 cubes rotated around their axis. It generates a very large number of co-planar facets, stressing both the

arithmetic kernel and the constrained Delaunay triangulation. Our result is shown in Figure 17-A (with co-planar facets simplification) and B (without co-planar simplification). The two CGAL-based kernels (C and D) produce a correct result (but it is not a Delaunay triangulation), and the “manifold” kernel fails producing a correct result for this specific example, as well as other ones with similar co-planar configurations or high mesh density.

In table 4, timings are reported for larger datasets, such as the union and difference of sphere with 200 Stanford bunnies with a Fibonacci distribution displayed on the first page. Each bunny has 75K vertices. The table also reports timings for the union of 200 spheres of various resolution (between 200 and 125K vertices). For the largest example, `fibonacci_sphere_500`, where the input has 62.5M vertices, the CGAL corefinement kernel crashed (out of memory). The “manifold” kernel did output a result in 385s, but this result has many missing triangles.

4 CONCLUSIONS

To conclude this article, I shall report some lessons I learned from this project, as well as possible directions for future work. What I find important to remember about this experience is the following list. Most elements will probably be not a big surprise, but I found it worth mentioning them:

- Non-regression testing is, as always, extremely important, especially for this algorithm, that has many parts, and each part is complicated;
- assertion checks everywhere in the code (e.g., testing the combinatorial consistency of the 3-Map, the Delaunay property of the triangulation) helps a lot detecting bugs at an early stage;
- Thingi10K is interesting, with such a large database, many corner cases are likely to happen, such as projection axis requiring exact precision #356074, 3D grid of mutually intersecting triangles that generate a huge number of intersections #996816 stressing the constrained Delaunay triangulation code, or mesh with a large number of very skinny triangles mutually intersecting around a pole #101633 stressing the arithmetic kernel. Solving these issues helped identifying hot spots that would have remained hidden otherwise;
- the arithmetic kernel can be stressed a lot by some meshes. Carefully optimizing the arithmetic kernel can be a key for optimal performance. The “complexity of the coordinates” impacts performance a lot, in particular with arithmetic expansions, but not only. For the predicates, use expressions that are as simple as possible, and compress often;
- a predicate can have different equivalent expressions. One can use one of them for the filter, another one for the exact evaluation and a third one for the symbolic perturbation;
- arithmetic expansions can be pushed a little bit, but soon one reaches their two limitations: (1) with cascaded constructions / predicates, exponents can overflow; (2) operations start to cost a lot with expansions longer than a few tenths of components. As soon as constructions are involved, multi-precision seems to be a better solution;

- implementing some well known algorithms, such as a 2D constrained Delaunay triangulation with intersecting constraints is delicate. Often, the main algorithm is simple, just as in the textbook, but most of the textbooks and existing references make simplifying assumptions (e.g., points in generic positions). For instance, in a 2D constrained Delaunay triangulation, detecting the edges that intersect a constraint with all the possible corner cases much subtler than one would think in the first place;
- exact constructions combined with exact predicates with interval filters appears to be a reasonable option for mesh intersection, which I was not sure when starting this project. This is probably because in a (not too convoluted) mesh with N elements, there are approximately \sqrt{N} elements in the intersection. One can afford paying more for these elements, because in general their number does not grow too quickly in function of N (except for #996816 of course !);
- the “simply implement the math” vision is nearly achievable. One can write elegant code that looks like the textbook algorithm, but this comes at the expense of carefully optimizing and treating all the corner cases in the arithmetic kernel, constructions and predicates. From a software engineering point of view, doing so is interesting because the most complicated code is confined into easy-to-test functions with a well defined API.

This work can be improved and extended in several directions. Clearly, the main missing component is a “snap rounding” algorithm, that transforms the exact coordinates into floating point numbers while preserving some topological properties. The approach described in [8, 47] is very promising. Another interesting direction is the approach completely based on floating-point numbers described in [19, 41]. It is a completely different paradigm. While the “manifold” OpenSCAD kernel, based on this paradigm, does not always output a correct result, it does very often, at a spectacular speed. It is very rare that it takes more than 1s for a CSG. Is it possible to derive an algorithm with the same performance and more guarantees ? Finally, it may be interesting to enrich the ThingiCSG database introduced in this article with a larger set of examples, especially if a larger research community wants to tackle this type of problems.

ACKNOWLEDGEMENTS

This work is supported by the COSMOGRAM Inria exploratory action (AeX). I wish to thank Nicolas Ray for discussions, and for always encouraging me to explore the simplest solution first, such as the global vertex map.

REFERENCES

- [1] Marco Attene. 2020. Indirect Predicates for Geometric Constructions. *Computer-Aided Design* 126 (2020), 102856. <https://doi.org/10.1016/j.cad.2020.102856>
- [2] Yves Bertrand and Jean-François Dufourd. 1994. Algebraic Specification of a 3D-Modeler Based on Hypermaps. *CVGIP Graph. Model. Image Process.* 56, 1 (1994), 29–60. <https://doi.org/10.1006/CGIP.1994.1005>
- [3] Guillaume Caumon, Charles H. Sword, and Jean-Laurent Mallet. 2003. Constrained modifications of non-manifold B-reps. In *Proceedings of the Eighth ACM Symposium on Solid Modeling and Applications 2003, Seattle, Washington, USA, June 16 - 20, 2003*, George Turkiyyah, Pere Brunet, Gershon Elber, and Vadim Shapiro (Eds.). ACM, 310–315. <https://doi.org/10.1145/781606.781657>

- [4] Gianmarco Cherchi, Marco Livesu, Riccardo Scateni, and Marco Attene. 2020. Fast and Robust Mesh Arrangements Using Floating-Point Arithmetic. *ACM Trans. Graph.* 39, 6, Article 250 (nov 2020), 16 pages. <https://doi.org/10.1145/3414685.3417818>
- [5] Gianmarco Cherchi, Fabio Pellacini, Marco Attene, and Marco Livesu. 2022. Interactive and Robust Mesh Booleans. *ACM Trans. Graph.* 41, 6, Article 248 (nov 2022), 14 pages. <https://doi.org/10.1145/3550454.3555460>
- [6] Christophe Delage and Olivier Devillers. 2004. Spatial Sorting. http://doc.cgal.org/latest/Spatial_sorting/index.html.
- [7] Olivier Devillers and Philippe Guigue. 2002. *Faster Triangle-Triangle Intersection Tests*. Technical Report RR-4488. INRIA. <https://inria.hal.science/inria-00072100>
- [8] Olivier Devillers, Sylvain Lazard, and William J. Lenhart. 2018. 3D Snap Rounding. In *34th International Symposium on Computational Geometry (SoCG 2018) (Leibniz International Proceedings in Informatics (LIPIcs), Vol. 99)*, Bettina Speckmann and Csaba D. Tóth (Eds.). Schloss Dagstuhl-Leibniz-Zentrum fuer Informatik, Dagstuhl, Germany, 30:1–30:14. <https://doi.org/10.4230/LIPIcs.SocG.2018.30>
- [9] Lorenzo Diazzi, Daniele Panozzo, Amir Vaxman, and Marco Attene. 2023. Constrained Delaunay Tetrahedrization: A Robust and Practical Approach. *ACM Trans. Graph.* 42, 6, Article 181 (dec 2023), 15 pages. <https://doi.org/10.1145/3618352>
- [10] Herbert Edelsbrunner and Ernst P. Mücke. 1994. Simulation of simplicity: a technique to cope with degenerate cases in geometric algorithms. *CoRR abs/math/9410209* (1994). [arXiv:math/9410209](http://arxiv.org/abs/math/9410209)
- [11] Paul-Louis George, Frédéric Hecht, and E. Saltel. 1990. Fully automatic mesh generator for 3D domains of any shape. *IMPACT Comput. Sci. Eng.* 2, 3 (1990), 187–218. [https://doi.org/10.1016/0899-8248\(90\)90012-Y](https://doi.org/10.1016/0899-8248(90)90012-Y)
- [12] Miguel Granados, Peter Hachenberger, Susan Hert, Lutz Kettner, Kurt Mehlhorn, and Michael Seel. 2003. Boolean Operations on 3D Selective Nef Complexes: Data Structure, Algorithms, and Implementation. In *Algorithms - ESA 2003*, Giuseppe Di Battista and Uri Zwick (Eds.). Springer Berlin Heidelberg, Berlin, Heidelberg, 654–666.
- [13] Less Hall. 2014. OpenSCAD presentation. <https://www.thingiverse.com/thing:325400>
- [14] Yixin Hu, Teseo Schneider, Bolun Wang, Denis Zorin, and Daniele Panozzo. 2020. Fast Tetrahedral Meshing in the Wild. *ACM Trans. Graph.* 39, 4, Article 117 (aug 2020), 18 pages. <https://doi.org/10.1145/3386569.3392385>
- [15] Yixin Hu, Qingnan Zhou, Xifeng Gao, Alec Jacobson, Denis Zorin, and Daniele Panozzo. 2018. Tetrahedral Meshing in the Wild. *ACM Trans. Graph.* 37, 4, Article 60 (jul 2018), 14 pages. <https://doi.org/10.1145/3197517.3201353>
- [16] Konstantinos Katrioplas, Sebastien Lorient, Mael Rouxel-Labbé, Jane Tournois, and Ilker O. Yaz. 2017. CGAL Polygon Mesh Processing - Corefinement and boolean operations. https://doc.cgal.org/latest/Polygon_mesh_processing/index.html#Coref_section.
- [17] Donald E. Knuth. 1997. *The Art of Computer Programming, Volume 2: Seminumerical Algorithms* (third ed.). Addison-Wesley, Boston.
- [18] Pierre Kraemer, David Cazier, and Dominique Bechmann. 2007. Multiresolution half-edges. In *Proceedings of the 23rd Spring Conference on Computer Graphics, SCCG 2007, Budmerice, Slovakia, April 26-28, 2007*, Mateu Sbert and Stephen N. Spencer (Eds.). ACM, 199–206. <https://doi.org/10.1145/2614348.2614376>
- [19] Emmett Lalish. 2022. Manifold: a library dedicated to creating and operating on manifold triangle meshes. <https://github.com/elalish/manifold>.
- [20] Capucine Legentil, Jeanne Pellerin, Paul Cupillard, Algiane Froehly, and Guillaume Caumon. 2022. Testing scenarios on geological models: Local interface insertion in a 2D mesh and its impact on seismic wave simulation. *Comput. Geosci.* 159 (2022), 105013. <https://doi.org/10.1016/j.cageo.2021.105013>
- [21] Bruno Levy. 2015. Geogram. *GitHub repository*. URL: <https://github.com/BrunoLevy/geogram> (2015).
- [22] Bruno Lévy. 2015. A Numerical Algorithm for L_2 Semi-Discrete Optimal Transport in 3D. *ESAIM M2AN (Mathematical Modeling and Analysis)* (2015).
- [23] Bruno Lévy. 2016. Robustness and efficiency of geometric programs: The Predicate Construction Kit (PCK). *Comput. Aided Des.* 72 (2016), 3–12. <https://doi.org/10.1016/j.cad.2015.10.004>
- [24] Bruno Lévy, Roya Mohayaee, and Sebastian von Hausegger. 2021. A fast semi-discrete optimal transport algorithm for the unique reconstruction of the early Universe. *Mon. Not. R. Astron. Soc.* (2021).
- [25] Pascal Lienhardt. 1988. Extension of the Notion of Map and Subdivisions of a Three-Dimensional Space. In *STACS 88, 5th Annual Symposium on Theoretical Aspects of Computer Science, Bordeaux, France, February 11-13, 1988, Proceedings (Lecture Notes in Computer Science, Vol. 294)*, Robert Cori and Martin Wirsing (Eds.). Springer, 301–311. <https://doi.org/10.1007/BFB0035854>
- [26] Pascal Lienhardt. 1994. N-Dimensional Generalized Combinatorial Maps and Cellular Quasi-Manifolds. *Int. J. Comput. Geom. Appl.* 4, 3 (1994), 275–324. <https://doi.org/10.1142/S0218195994000173>
- [27] Marco Livesu, Gianmarco Cherchi, Riccardo Scateni, and Marco Attene. 2022. Deterministic Linear Time Constrained Triangulation Using Simplified Earcut. *IEEE Transactions on Visualization and Computer Graphics* 28, 12 (2022), 5172–5177. <https://doi.org/10.1109/TVCG.2021.3070046>
- [28] Adrien Loseille and Frédéric Alauzet. 2009. Optimal 3D Highly Anisotropic Mesh Adaptation Based on the Continuous Mesh Framework. In *Proceedings of the 18th International Meshing Roundtable, IMR 2009, October 25-28, 2009, Salt Lake City, UT, USA*, Brett W. Clark (Ed.). Springer, 575–594. https://doi.org/10.1007/978-3-642-04319-2_33
- [29] Max Lyon, David Bommers, and Leif Kobbelt. 2016. HexEx: robust hexahedral mesh extraction. *ACM Trans. Graph.* 35, 4 (2016), 123:1–123:11. <https://doi.org/10.1145/2897824.2925976>
- [30] Bruno Lévy. 2022. Partial optimal transport for a constant-volume Lagrangian mesh with free boundaries. *J. Comput. Phys.* 451 (2022), 110838. <https://doi.org/10.1016/j.jcp.2021.110838>
- [31] David J. MacDonald and Kellogg S. Booth. 1990. Heuristics for ray tracing using space subdivision. *Vis. Comput.* 6, 3 (may 1990), 153–166. <https://doi.org/10.1007/BF01911006>
- [32] Jean-Laurent Mallet. 2002. *Geomodelling*.
- [33] Andreas Meyer and Sylvain Pion. 2008. FPG: A code generator for fast and certified geometric predicates. In *Real Numbers and Computers*. Santiago de Compostela, Spain, 47–60. <https://inria.hal.science/inria-00344297>
- [34] Ole Møller. 1965. Quasi double-precision in floating point addition. *BIT* 5, 1 (mar 1965), 37–50. <https://doi.org/10.1007/BF01975722>
- [35] Farnik Nikakhtar, Ravi K. Sheth, Bruno Lévy, and Roya Mohayaee. 2022. Optimal Transport Reconstruction of Baryon Acoustic Oscillations. *Phys. Rev. Lett.* 129, 25, Article 251101 (Dec. 2022), 251101 pages.
- [36] Jeanne Pellerin, Arnaud Botella, François Bonneau, Antoine Mazuyer, Benjamin Chauvin, Bruno Lévy, and Guillaume Caumon. 2017. RINGMesh: A programming library for developing mesh-based geomodelling applications. *Computers & Geosciences* 104 (2017), 93–100. <https://doi.org/10.1016/j.cageo.2017.03.005>
- [37] Jonathan Richard Shewchuk. 1996. Robust Adaptive Floating-Point Geometric Predicates. In *Proceedings of the Twelfth Annual Symposium on Computational Geometry*. Association for Computing Machinery, 141–150.
- [38] Jonathan Richard Shewchuk. 1996. Triangle: Engineering a 2D Quality Mesh Generator and Delaunay Triangulator. In *Applied Computational Geometry: Towards Geometric Engineering*, Ming C. Lin and Dinesh Manocha (Eds.). Lecture Notes in Computer Science, Vol. 1148. Springer-Verlag, 203–222. From the First ACM Workshop on Applied Computational Geometry.
- [39] Jonathan Richard Shewchuk. 1997. Adaptive Precision Floating-Point Arithmetic and Fast Robust Geometric Predicates. *Discrete & Computational Geometry* 18, 3 (Oct. 1997), 305–363.
- [40] S. W. Sloan. 1992. A fast algorithm for generating constrained Delaunay triangulation. *Comput. & Structures* (1992).
- [41] Julian Smith and Neil Dodgson. 2006. A Topologically Robust Boolean Algorithm Using Approximate Arithmetic. In *Proceedings of the 22nd European Workshop on Computational Geometry*.
- [42] Charles H. Sword. 1996. Cut Algorithm: old and new. In *Proc. 13th Gocad Meeting, Nancy*.
- [43] Pierre Terdiman. 2001. Memory-optimized bounding-volume hierarchies. <http://www.codercorner.com/Opcode.pdf>.
- [44] Pierre Terdiman. 2001. Zero-bytes AABB Trees. <http://www.codercorner.com/ZeroByteBVH.pdf>.
- [45] The CGAL Project. 2023. *CGAL User and Reference Manual* (5.5.2 ed.). CGAL Editorial Board. <https://doc.cgal.org/5.5.2/Manual/packages.html>
- [46] The CGAL Project. 2023. *CGAL User and Reference Manual* (5.5.2 ed.). CGAL Editorial Board. <https://doc.cgal.org/5.5.2/Manual/packages.html>
- [47] Leo Valque. 2019. *3D Snap Rounding*. Master’s thesis. Université de Lyon. <https://inria.hal.science/hal-02393625>
- [48] Sebastian von Hausegger, Bruno Lévy, and Roya Mohayaee. 2022. Accurate Baryon Acoustic Oscillations Reconstruction via Semidiscrete Optimal Transport. *Phys. Rev. Lett.* 128, 20, Article 201302 (May 2022), 201302 pages.
- [49] Kevin Weiler. 1985. Edge-Based Data Structures for Solid Modeling in Curved-Surface Environments. *IEEE Computer Graphics and Applications* 5, 1 (1985), 21–40. <https://doi.org/10.1109/MCG.1985.276271>
- [50] Kevin Weiler. 1988. The radial edge data structure: a topological representation for non-manifold geometric boundary modeling. In *Geometric modeling for CAD applications: selected and expanded papers from the IFIP WG 5.2 working conference*, M.J. Wozny and H.W. McLaughlin (Eds.). Elsevier, 3–36.
- [51] Claire Wolf and OpenSCAD contributors. 2010. OpenSCAD. <https://openscad.org/>.
- [52] Qingnan Zhou and Alec Jacobson. 2016. Thingi10K: A Dataset of 10,000 3D-Printing Models. *arXiv preprint arXiv:1605.04797* (2016).

A ONLINE RESOURCES

- The algorithm with the expansion-based kernel and the CSG parser are available in the geogram library [21] here: <https://github.com/BrunoLevy/geogram>
- Thingi10K: <https://ten-thousand-models.appspot.com/>, [52]